University Politehnica of Bucharest

Doctoral School of Applied Chemistry and Materials Science

Mesoporous silica-based composites for controlled release of biologically active molecules

---

Compozite pe bază de silice mezoporoasă în sisteme cu eliberare controlată de substanțe biologic active

PhD THESIS SUMARY

Scientific leader : Prof. dr. ing. Daniela Berger

Author : Marilena Georgescu (Petrescu)

Bucharest
2017

Keywords: drug delivery systems, mesoporous silica, silica-ceria composite, aluminosilicate, functionalized mesoporous silica, alginate beads, magnetite-aluminosilicate composites, doxycycline, oxyteracycline, ketoprofen, doxorubicin

Contents

The list of abbreviations

MCM-41	Mobil Composition of Mater no. 41
SBA	Santa Barbara Amorphous
APTES	3-aminopropyltriethoxysilane
AlSBA-16	aluminosilicate from SBA class
BuDEA	butyldiethanolamine
$Al(BuO)_3$	aluminum tributoxide
TEOS	tetraethyl orthosilicate
S_{BET}	specific surface area calculated with the BET method
d_{BJH}	average pore diameter calculated by Barrett Joyner Halenda method
XRD	X-ray diffraction
DSC	differential scanning calorimetry
SEM	scanning electron microscopy
TEM	transmission electron microscopy
BSE	back-scattered electron detector
EDX	Energy dispersive X-Ray
a. u.	arbitrary units
HMS	Hexagonal Mesoporous silica
MSU	Michigan State University

I.1. Introduction

The discovery of silica-type mesoporous materials in the 90s was of a particular interes for researchers due to their properties, which recommend them for applications in chromatographic separations, catalysis, molecules adsorption etc, their most promising being in the field of biomedice. In 2001, mesoporous silica MCM-41 was proposed as a carrier in drug delivery systems due to its outstanding properties: an ordered pore framework with narrow pore size distribution, large total pre volume for accommodation of required amount of drug molecules, high specific surface, the presence of silanol groups involved in the post-synthesis functionalization for the modification of silica surface properties in order to tailor the interactions between the support and guest molecles for a desired delivery kinetics.

To enhance mesoporous silica carrier should interact with biologically active substances. This can be achieved by tuning the properties of carrier using two strategies: either through the carrier synthesis conditions, especially in order to obtain a pore size suitable for the adsorption of organic molecules or by the functionalization of silica surface with different organic groups

The research reported in this PhD thesis consists in the development of drug delivery systems based on mesoporous matrix carriers, silica, aluminosilicates, silica-ceria and magnetite-aluminosilicate composites. In this regard, different mesoporous materials were synthesized, characterized and tested as carriers for tetracyclines (oxytetracycline and doxycycline), anti-inflammatory (ketoprofen) and cytostatic agent (doxorubicin).

The PhD thesis consists of two parts: Part I comprises literature data in three chapters. Chapter 1 deals with the basic knowledge concerning the mesoporous silica and aluminosilicates used as vehicles in drug delivery systems. Chapter 2 describes the obtaining methods of mesoporous silica, functionalization approaches, the effect of introduction aluminum in the silica framework on the structural and textural material parameters, composites based mesoporous silica, and drug delivery systems based on alginate beads. Chapter 3 presents some literature data about the biologically active substances used in this thesis, chosen as model molecules from the tetracyclines, anti-inflammatories and cytostatic class.

Part II describes the original contributions and contains five chapters. Chapter 1 presents the justification of topic chosen and the scope and the objectives of the thesis. Chapter 2 is dedicated to the first two objectives, namely, the synthesis and characterization of several inorganic mesostructured materials, obtaining functionalized mesoporous silica samplesf by the post-synthesis approach. Chapters 3 and 4 comprise the developed drug delivery systems based on MCM-41-type supports, containing antibiotics. Chapter 5 is focused on the fulfillment of the fourth objective and presents the development of ketoprofen delivery systems obtained by the encapsulation of silica-ketoprofen-type composites in alginate beads. Chapter 6 describes the entrapment of doxorubicin in superparamagnetic magnetite-aluminosilicate-type composites and studies of drug release profiles in the biological fluid that simulates the tumor cells environment, which consists in the last thesis objective.

The original results obtained during the doctoral studies were diseminated in four papers, three in the ISI journals (one in press) and one in UPB Scientic Bull. Series B, two conferences as posters at the Days of "Alexandru Ioan Cuza" University of Iasi, 2015 and PRIOCHEM XII - 2016, section 3 - Multifunctional Materials and Nanocomposites.

I. ORIGINAL CONTRIBUTIONS OBJECTIVES

The aim of this PhD thesis was the development of drug delivery systems based on inorganic carriers containing carriers based on mesoporous silica.

To fulfill the PhD thesis aim the following objectives were established:

1. Synthesis and characterization of several mesostructured silica-type materials
2. Synthesis and characterization of functionalized mesoporous silica materials using the post-synthesis approach
3. Development of antibiotics delivery systems containing inorganic transporters MCM-41
4. Developing complex drug delivery systems of ketoprofen by encapsulating silica-ketoprofen-type composites in alginate beads
5. encapsulation of doxorubicin in aluminosilicate-type inorganic composites and the study of release profiles of the therapeutic agent in biological fluid that simulates tumor cell environment.

To accomplish these objectives, the following activities were carried out:

- Synthesis of ceria-silica composites by two different methods, two types of silica functionalized with aminopropyl groups by post-synthesis, other types of silica and aluminosilicates for comparison and some magnetite-aluminosilicate composites.
- Characterization of mesoporous transporters synthesized by FTIR spectroscopy, wide- and small-angles XRD, N_2 adsorption-desorption isotherms recorded at 77K, SEM, TEM and thermal analysis.
- Preparation of composites based on doxycycline, oxytetracycline, ketoprofen and doxorubicin by incipient wetness impregnation method.
- Characterization of composites containing active biologic substances by FTIR spectroscopy, wide- and small-angles XRD, N_2 adsorption-desorption isotherms at 77 K.
- Perform *in vitro* release studies and fit experimental data with different functions to understand interactions between the transporter and the drug and the type of transport that accompanies the desorption of organic molecules.
- Encapsulation of ketoprofen-silica materials in alginate beads and determination of *in vitro* release profiles of ketoprofen from these complex carriers.
- Determination of antimicrobial activity for antibiotics and proliferation and cell death tests on healthy human lymphocytes for doxorubicin encapsulated in magnetite-aluminosilicate type transporters as compared to treatment with cytostatic agent solution at the same concentration.

II.2. Carriers based on mesoporous silica

A first objective of the research was the obtaining of mesoporous silica-based materials, aluminosilicates, ceria-silica and magnetite-aluminosilicate composites by sol-gel method, which were further applied as carriers in drug delivery systems. For the first time, mesoporous ceria-silica composites have been investigated as carriers in drug delivery systems. Two synthesis methods were chosen for obtaining mesoporous silica-ceria composites: *(i)* two-step synthesis that first involves the synthesis of ceria nanoparticles by the hydrothermal method, and then their coating with MCM-41 mesoporous silica and *(ii)* one step method in which MCM-41 mesoporous silica was first precipitated, a solution containing corresponding cerium ions was added, and then the reaction mixture was hydrothermally treated. By this last method, two mesoporous silica-ceria composites with different concentrations of 10% (mol) and 20% (mol) ceria, labeled MCM-CeO_2 (1) and MCM-CeO_2 (2), respectively, were synthesized and characterized.

Several types of mesoporous silica synthesized according the procedures reported by our research group were chosen for comparison: a mesoporous MCM-41 silica sample, for which the surfactant was removed by either by extraction or calcination at 550ºC/5h [27,28], AlMCM-41 (Si/Al=51) synthesized in the presence of C_{14}TAB [30] and two MCM-48 silica samples with different textural properties because of different structure directing agents used, C_{16}TAB and

GEMINI 16-12-16 [31]. Also for this study were chosen commercially available materials: AlMCM-41 (Si/Al = 40, Sigma) and MCM-41 (Sigma).

Also, mesoporous silica-ceria composites were compared with two types of functionalized mesoporous silica with 3-aminopropyl groups, MCM-APTES and MCF-APTES obtained by the post-synthesis method. The synthesis and characterization of functionalized silica materials represent the second objective of the thesis.

Also, magnetite-aluminosilicate composites (Fe_3O_4@AlMCM-41, Fe_3O_4@ AlMCM-PEG, Fe_3O_4@AlSBA-15) and SBA-APTES-FOLATE material were also tested for doxorubicin, a cytostatic agent for the development of targeted drug delivery systems.

The synthesized mesoporous materials were characterized by small and wide-angle X-ray powder diffraction, FTIR spectroscopy and nitrogen adsorption-desorption isotherms, SEM, TEM, thermal analysis. The specific surface values were determined using the Brunauer-Emmet-Teller (BET) model in the 0,05-0,30 relative pressure range from the adsorption isotherm branch, while the pore size distribution curves for the prepared materials were computed from the desorption branch by using the Barrett-Joyner-Halenda theory (BJH).

In order to determine the morphology of mesoporous materials, they were investigated by SEM and TEM. Thermal analysis (DTA-TG) was performed in air, using alumina crucibles at a heating rate of 10°C/min from 20º-1000ºC. Si/Al molar ratio values of aluminosilicate samples were calculated based on EDX analyses performed in at least five different sample regions.

In the FTIR spectra of the carriers (Figures II.9 and II.10) one can observe the characteristic bands of each mesoporous material.

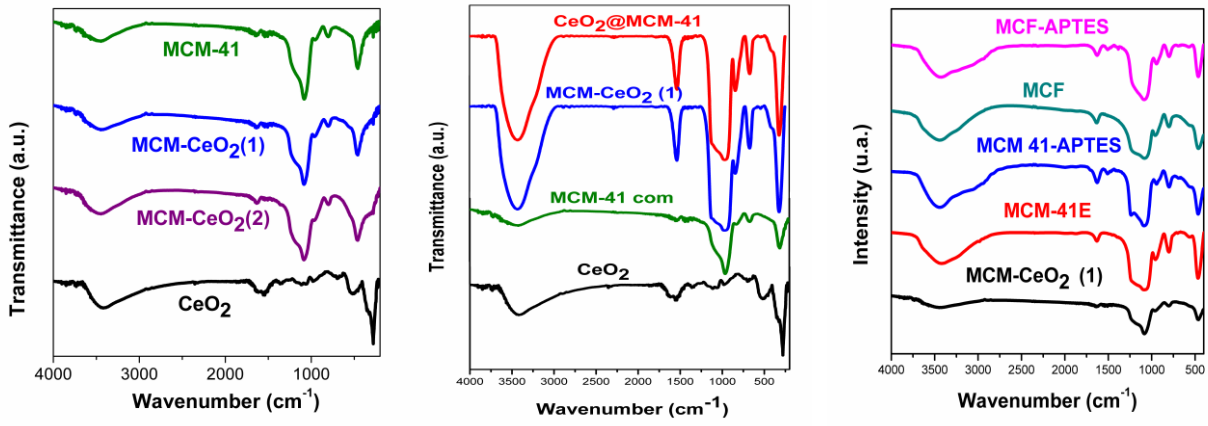

(A) (B) (C)

Fig. II.9. FT-IR spectra of: silica-ceria composites compared to CeO_2 (A și B) and silica type of MCM-41 and MCF pristine and functionalized with APTES (C) samples

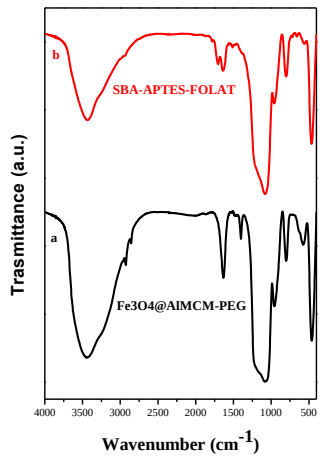

Fig.II.10 FT-IR spectra of supports: (a) Fe_3O_4@AlMCM-PEG și (b) SBA-APTES-FOLAT

The formation of crystalline cubic fluorite structure for CeO_2 (Fig.II.11.A și Fig.II.12.A) phase in all silica-ceria composite materials was evidenced by wide-angle XRD. An amorphous silica phase is also presented in the core-shell silica-ceria composite material. Furthermore, the intensity of the CeO_2 diffraction peaks is reduced for the CeO_2@MCM-41, MCM-CeO_2 materials with respect to CeO_2 nanoparticles, as expected because the weight fraction decrease of the ceria cubic phase in these composite materials.

The small-angle XRD (Fig.II.11.B și Fig. II.12.B) demonstrate that both core-shell and ceria-silica composite materials present ordered pore arrays, characteristic for MCM-41 silica.

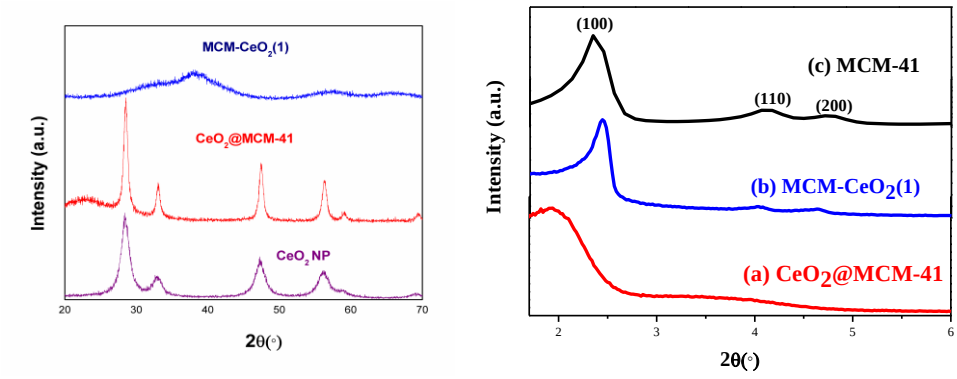

(A) (B)

Fig. II.11. Wide-angle XRD (A) patterns of CeO_2-based carriers and the small-angle XRD (B) patterns of CeO_2-based carriers in comparision with MCM-41

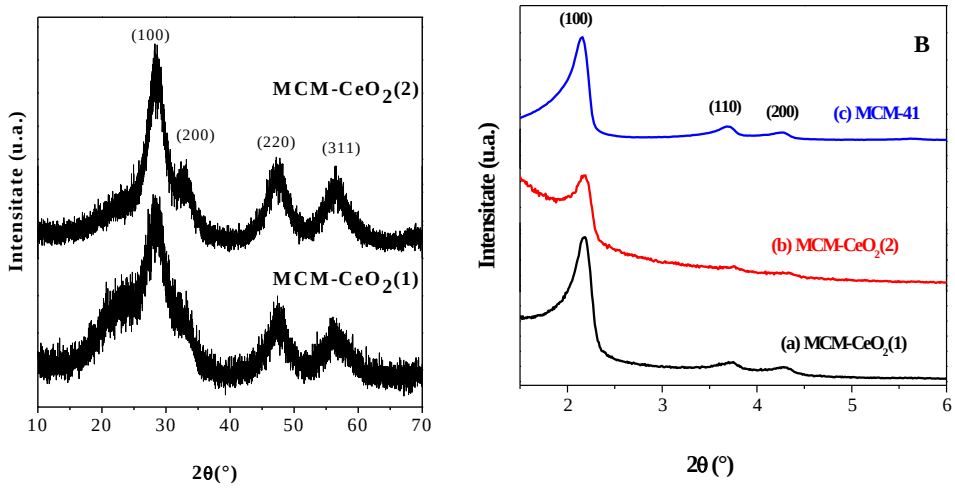

(A) (B)

Fig. II.12. XRD patterns of silica-ceria composites calcined at 550°C/5h: wide angle (A) and small angle in comparison with MCM-41 (B)

The small-angle XRD for the mesoporous silica and aluminosilicate samples showed the formation of mesostructured materials with a hexagonal pore framework belonging to the *p6m* space group symmetry. All samples have at least three Bragg reflections characteristic for MCM-41-type materials.

The wide-angle XRD for composite materials containing magnetite nanoparticles (Fig. II.13.a) demonstrated the preservation of diffraction peaks of magnetite phase, as well as the formation of the wide peak characteristic for amorphous silica.

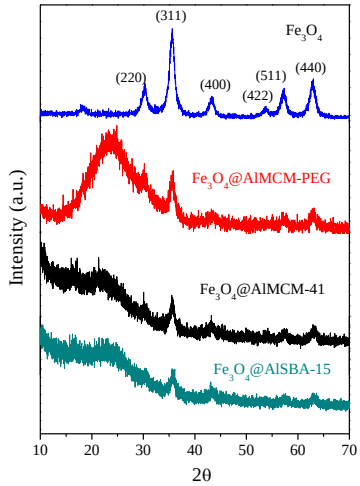

Fig.II.13. Wide-angle XRD patterns (a) for the materials containing magnetite nanoparticles

The morphology of mesoporous carriers was investigated by SEM (Fig. II.14, Fig. II.15.B, C, D și Fig. II.18) and TEM investigation (Fig. II.15.A, Fig.II.16 și Fig. II.17).

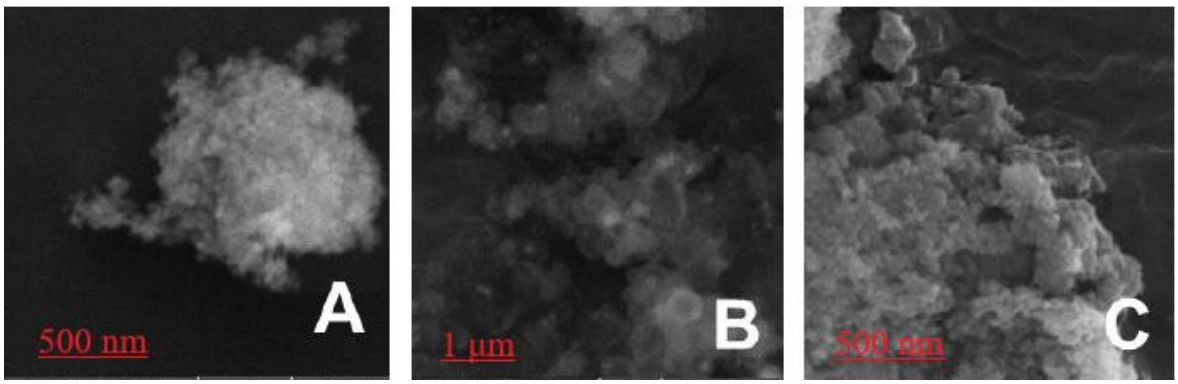

Fig.II.14. SEM micrographs of CeO_2 NP (A), CeO_2@MCM-41(B) and MCM-CeO_2 (C)

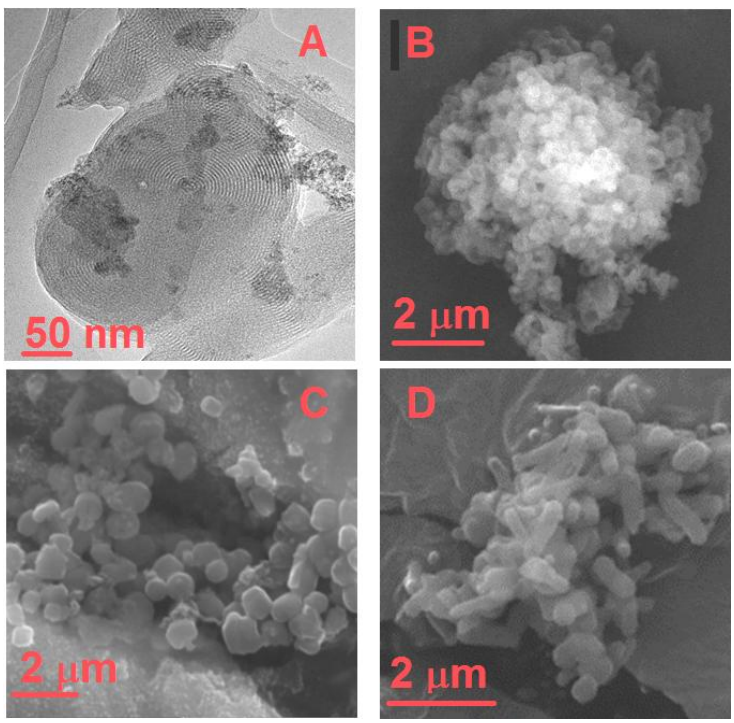

Fig. II.15. TEM image for MCM-CeO_2 (1)(A) and SEM micrographs for MCM-CeO_2 (2) (B), MCM-41 sample, calcined at 550°C (C) and MCM-41E samples(D)

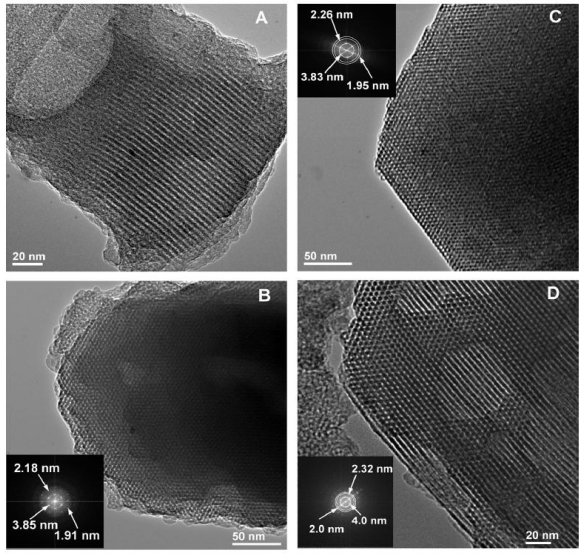

Fig.II.16 TEM image for MCM-41E (A și B), AlMCM-41E (42) (C) and AlMCM-41 (22) (D). Insert the FFT images.

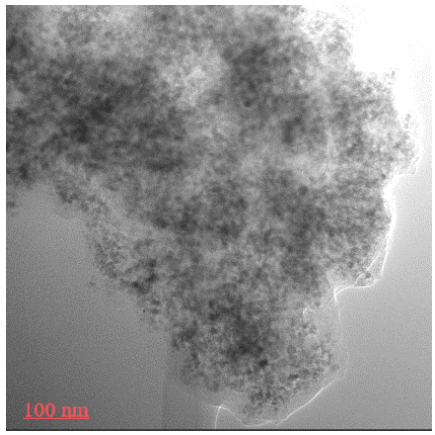

Fig. II.17. TEM image for Fe_3O_4-AlSBA-15 material

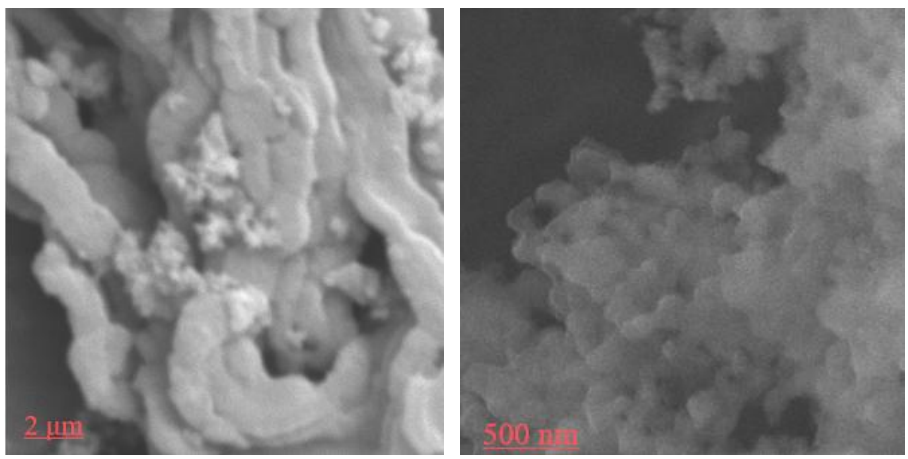

A B

Fig. II.18. SEM image for Fe_3O_4@AlSBA-15 (A) and Fe_3O_4@AlMCM-41(B)

The N_2 adsorption-desorption isotherms of silica-ceria composites demonstrated relatively high porosity, being type IV, characteristic for mesoporous materials, except for ceria nanoparticles that showed no porosity, its isotherm being type II (Fig.II.19, Fig. II.20, Fig. II.21 și Fig. II.22).

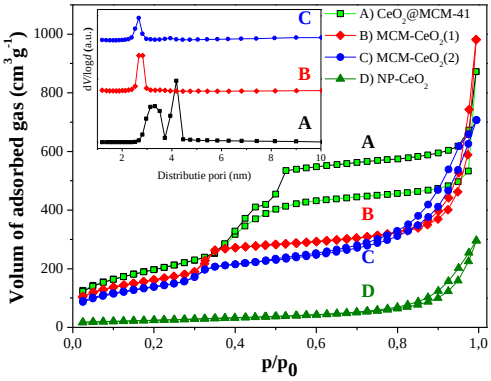

Fig. II.19. N_2 adsorption-desorption isotherms of: CeO_2@MCM-41 (A), MCM-CeO_2 (1) (B) and CeO_2 NP (C)

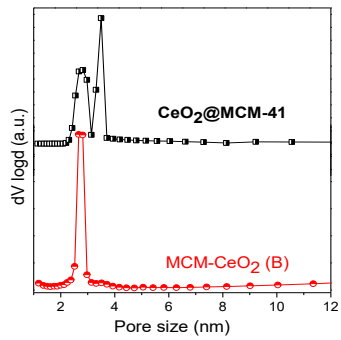

Fig. II.20. Pore size distribution curves for MCM-CeO_2 (1) (red curve) and CeO_2@MCM-41 (1)

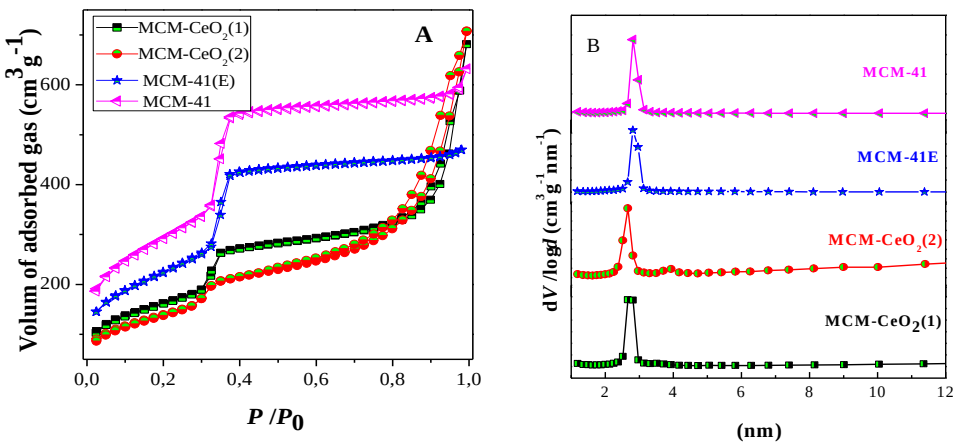

Fig. II.21. N_2 adsorption-desorption isotherm of: MCM-CeO_2 (1) , MCM-CeO_2 (2), MCM -41 and MCM-41E (A) and pore size distribution (B)

The textural parameters (specific surface area, S_{BET}, total pore volume, V_p, and average pore diameter, d_{BJH}) of the carriers, determined from N_2 adsorption-desorption isotherms are presented in the Tables II.3- II.5.

Table II.3. Textural parameters of silica-ceria composites in comparison with those of MCM-41-type silica and ceria samples

Sample	d_{BJH} (nm)	S_{BET} (m^2g^{-1})	V_{pore} (cm^3g^{-1})
MCM-41 (Sigma)	3,0	959	0,91
CeO_2 NP	-	88	0,10
CeO_2@MCM-41	3,30	717	1,40
MCM-CeO_2 (1)	2,66	683	0,67
MCM-CeO_2 (2)	2,67	512	1,14
MCM-41E	2,82	818	0,78

MCM-41 (550°C)	2,82	1039	1,06

Table. II.4. Synthesis conditions, structural and the textural properties for mesoporous silica and aluminosilicate supports

Support (Si/Al molar ratio)	Synthesis conditions	d_{100} (nm)	a_0 (nm)	wt (nm)	S_{BET} (m^2/g)	V_{pore} (cm^3/g)	d_{BJH} (nm)
MCM-41E	C_{16}TAB	4,060	4,688	1,87	819	0,73	2,82
MCM-41	Comercial	4,105	4,740	1,98	1010	0,99	2,76
AlMCM-41E(51)	C_{14}TAB, Al(O^{sec}Bu), 600 ºC	3,620	4,180	1,61	836	0,87	2,57
AlMCM-41 (40)	Comercial	3,914	4,520	1,64	824	0,81	2,88
MCM-48	C_{16}TAB, 600 ºC	-	8,93	0,69	1292	1,44	2,76
MCM-48G	Gemini, 600 ºC	-	8,04	0,83	854	0,97	2,26
MCM-APTES		-	-	-	585	0,51	2,39
MCF		-	-	-	876	2,49	10,40
MCF APTES		-	-	-	518	1,98	9,02

Table II.5. The textural parameters of magnetite-aluminosilica composites

Magnetic mesopous matrices	S_{BET} (m_2/g)	V_{pori} (cm^3/g)	d_{BJH} des (nm)	d_{BJH} ads (nm)
Fe_3O_4@AlMCM-41	609	0,57	2,66	2,66
Fe_3O_4@AlSBA-15	829	1,12 0.88 (d_{por}< 10 nm)	6,81	8,99

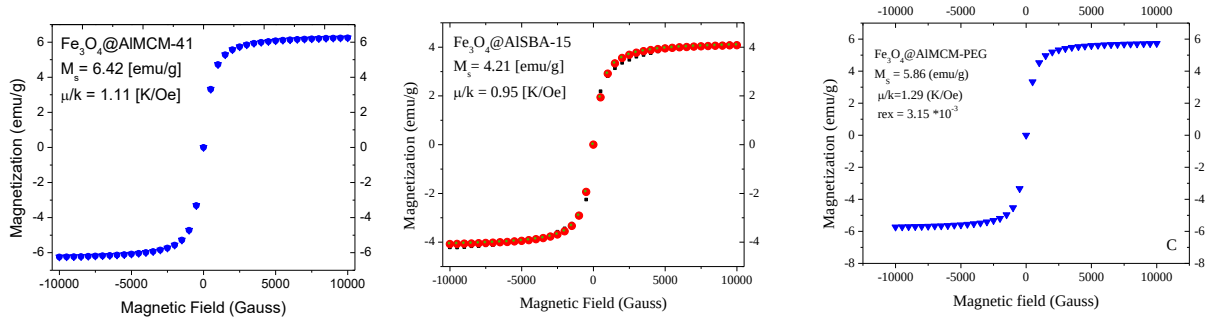

Fig. II.23. Magnetisation curve function of applied magnetic field for Fe_3O_4@AlMCM-41 (A), Fe_3O_4@AlSBA-15 (B) and Fe_3O_4@AlMCM-PEG (C) composites

The synthesized magnetite-aluminosilicate composites exhibit superparamagnetic behavior (Figure II.23) and high porosity, characteristics that recommend them to be tested as vehicles in targeted drug delivery systems.

Composites based on tetracyclines

The third objective of this thesis was the development of antibiotic delivery systems based on inorganic carriers such as: MCM-41 and MCM-48 silica, silica-ceria composites and aluminosilicates. Doxycycline and oxytetracycline were used as antibiotic molecules. The *in vitro* release studies and determination of antimicrobial activity of drug-loaded materials are presented in Chapters II.3 and II.4.

The antibiotics were adsorbed into the mesopores of silica-type carriers by incipient wetness impregnation method [32, 33], using silica-ceria composites and MCM-41 silica in the case of doxycycline and MCM-41, MCM-48, MCM-41-type silica-ceria composites with 10% (mol) and 20% (mol) ceria and aluminosilicates for oxytetracycline. The content of doxycycline drug-loaded silica-ceria composites was 25% (wt), as well as in Doxy1/MCM-41 material, while in the case of Doxy2/MCM-41 sample the content of drug was 40% (wt).

The antibiotic-loaded silica samples were investigated by small- and wide-angle XRD, FTIR spectroscopy and N_2 adsorption-desorption isotherms. The presence of antibiotics in all samples was evidenced by FT-IR spectroscopy (Fig.II.24. și Fig. II.29).

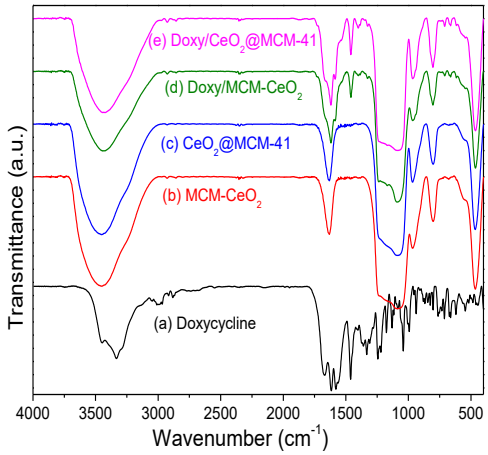

Fig. II.24. FT-IR spectra for: doxycycline, carriers (MCM-CeO_2, CeO_2@MCM-41) and doxycycline-loaded silica samples

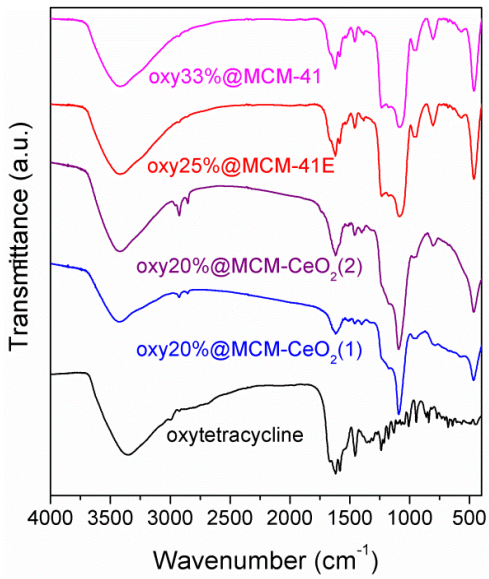

Fig.II.29. FTIR spectra of oxytetracycline-loaded silica-type supports and oxytetracycline

The vibrations of doxycycline can be noticed in the range of 1700-1300 cm^{-1} in the spectra of doxycline-loaded samples, besides the characteristic vibrations of carrier: Si-O-Si (1225, 1090, 465 cm^{-1}) and Si-OH (966 cm^{-1}) (Fig. II.24).

In the FTIR spectra of drug-loaded samples it can be observed the vibration bands that belong to the support, besides the ones of the drug located in the range of: 2850-2950 cm^{-1} attributed to $\vartheta_{as,s}$(CH)), 1590-1650 cm^{-1} ascribed to the deformation of amide moieties and 1310-1410 cm^{-1} assigned to the phenol groups (Fig. II.29).

Wide-angle XRD patterns of antibiotic-loaded materials (Figures II.25 and II.30) indicate that the drug molecules are adsorbed amorphous phase into the carrier mesopores due to the absence of antibiotic-specific Bragg reflections. The ordered pore array is preserved after the drug loading procedure, as the small-angle XRD patterns of the doxycycline-loaded silica-ceria composites showed (Fig. II.25-inset). In the wide-angle XRD patterns of the oxytetracycline-loaded samples (Fig. II.30), only the Bragg reflections of fluorite phase can be noticed, demonstrating that the antibiotic molecules were adsorbed into the carrier mesopores in amorphous state. The lack of oxytetracyclene diffraction peaks suggested that no crystalline drug was present on the surface of the drug-loaded samples, as it was expected.

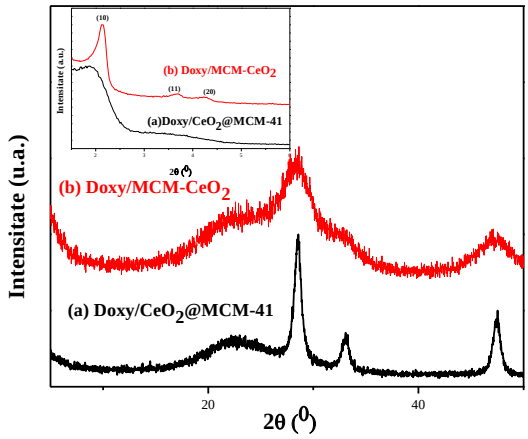

Fig. II.25. Wide-angle XRD patterns of doxycycline-loaded ceria-silica composites. Inset shows the small-angle XRD data for the same samples

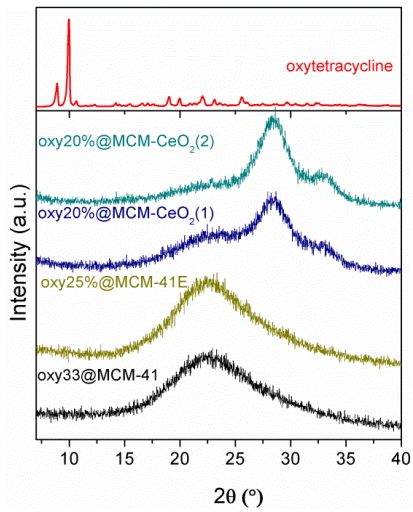

Fig.II.30 Wide-angle XRD patterns of representative oxytetracycline-loaded supports and oxytetracycline

All antibiotics-loaded materials exhibit type IV N_2 adsorption-desorption isotherm. (Fig. II.26 and II.32). The loading of therapeutic agent into the mesochannels is supported by the decrease of the pore volume and specific surface area values for the antibiotic-loaded composites (Tables II.6 and II.9). The adsorption of either doxycycline or oxytetracycline did not cause significant changes in the average pore size (Fig. II.26-inset and II.33), indicating poor interactions between the mesoporous carrier and the therapeutic agent were established. Oxitetracycline-loaded MCM-48 or MCM-48G supports showed that the adsorption of antibiotic molecules led to less ordered systems as small-angle XRD data demonstrated.

Table II.6. Textural parameters of doxycycline–loaded materials

Sample	Doxycycline (%)	d_{BJH} (nm)	S_{BET} (m^2g^{-1})	$V_{mezopore}$ (cm^3g^{-1})
Doxy/CeO_2@MCM-41	25	3.20	266	0.61
Doxy/MCM-CeO_2	25	2.70	269	0.19
Doxy/MCM-41	25	2.80	553	0.54
Doxy2/MCM-41	40	2.80	236	0.26

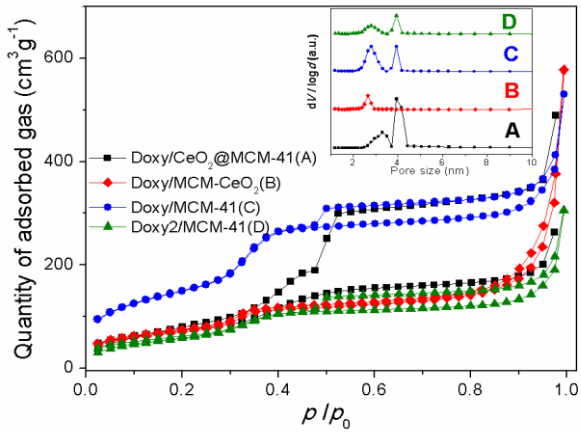

Fig. II.26. N_2 adsorption-desorption of doxycycline–loaded materials. Inset the pore size distribution curves for doxycycline-loaded materials

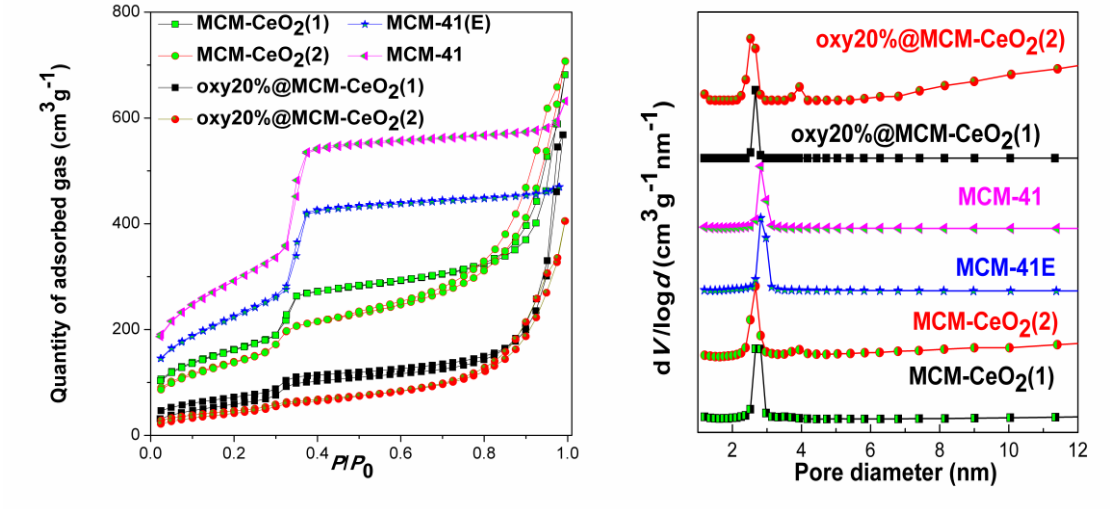

(A) (B)

Fig. II.32. N_2 adsorption-desorption isotherms recorded at liquid nitrogen temperature for the carriers in comparision with oxytetracycline samples (A) and their coresponding pore size distribution curves (B)

Tabelul II. 9.Textural parameters of representative oxytetracycline-loaded materials

Sample (Si/Al molar ratio)	S_{BET} (m^2/g)	V_{pori} (cm^3/g)	d_{BJH} (nm)
oxy20%@MCM-CeO_2(1)	265	0,05 (dp<10 nm)	2,64
oxy20%@MCM-CeO_2(2)	173	0,04 (dp<10 nm)	2,52
oxy25%@MCM-41E*	144	0,15 (dp<10 nm)	2,81
oxy33%@MCM-41*	163	0,10 (dp<10 nm)	2,80
oxy25%@AlMCM-41 (40)	398	0,27	2,39
oxy25%@AlMCM-41 (51)	311	0,15	2,25
oxy25%@MCM-48G	167	0,13	2,13

*for MCM-41E, the structure directing agent was removed by extraction, while for MCM-41 and aluminosilicates the surfactant was removed by clacination at 550ºC/5h.

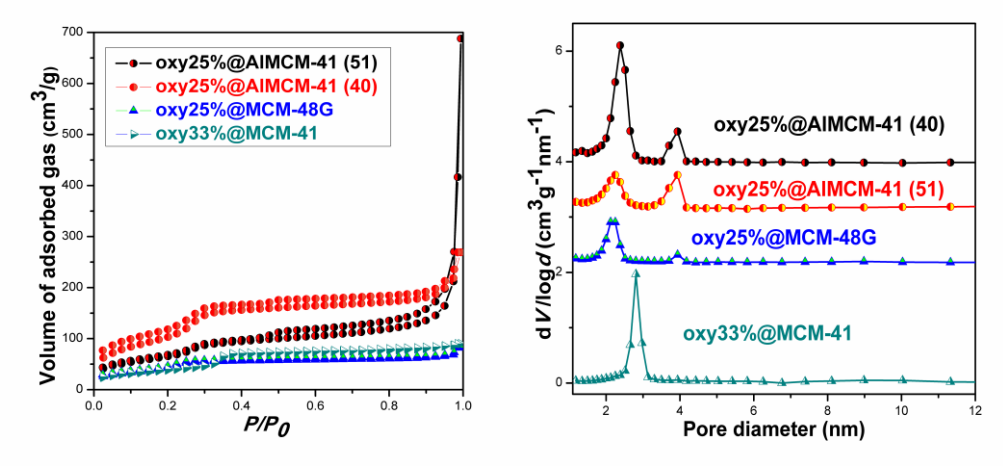

(A) (B)

Fig. II.33. N_2 adsorption-desorption of oxytetracycline-loaded materials (A) and their pore size distribution curves calculated with BJH model from the desorption branch of isotherms (B)

In vitro drug release experiments were performed at *p*H 5,5, close to the isoelectric *p*H of doxycycline, as the drug has the highest solution stability in these conditions [34].

Doxycycline dissolution at 37°C, *p*H 5,5 is almost complete after 15 minutes (Fig.II 28 D). The drug release from MCM-CeO_2 or MCM-41 silica is slower than the dissolution of the pure antibiotic, with ~95% drug released after 40 minutes. Interestingly, a lower doxycycline weight fraction leads to a faster release profile (Fig. II.28, E curve versus C curve), suggesting that the diffusion through the mesopores is the rate limiting step. The Doxy/MCM-CeO_2 hybrid material has the slowest release rate of the investigated materials (Fig. II.28 B). In the case of the core-shell carrier (Fig. II.28 A), the most drug molecules are released in the first 2 minutes, followed by a gradual decrease of drug concentration. This phenomenon could be explained by the adsorption of the active biological agent onto or close to the particle support surface, leading to an almost instantaneously release, as the drug diffusion length into the mesopores is significantly reduced. The subsequent doxycycline concentration decrease might indicate drug readsorption into the support mesochannels.

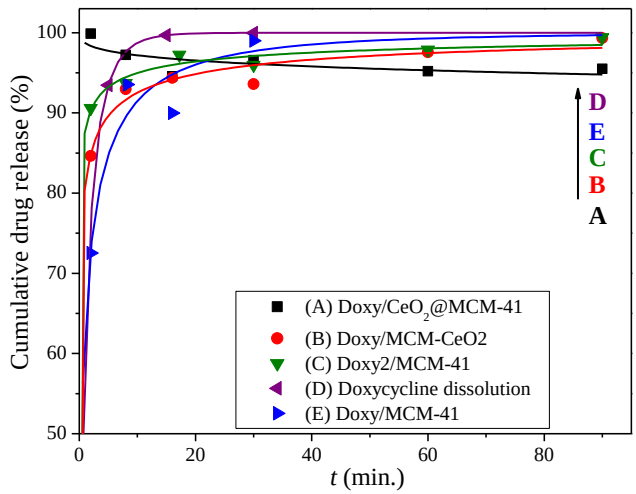

Fig.II 28. Doxycycline cumulative release from the core-shell (A) and composite (B) ceria-silica supports, MCM-41 silica (C, E) and doxycycline dissolution (D) at 37°C, *p*H 5,5. Symbols indicate experimental data points, lines indicate data fitted with the Weibull model.

The experimental release profiles were fitted using the Weibull model, a kinetic model based on the theory of percolation into fractal space.[35] The cumulative release *F* is expressed as a two-parameter exponential function of time: $M(t)/M(\infty) = 1 - exp(-at^b)$, where the *a* parameter is a measure of the release rate, while the *b* parameter indicates the ordering of the diffusion space, with

values greater than ~0.69 indicating diffusion in Euclidian space and lower values signifying diffusion in fractal space [36]. The Weibull model parameters (Table II.8) show that the release mechanism of the antibiotic molecules from silica and ceria-silica composites corresponds to diffusion in fractal space, as opposed to doxycycline dissolution (Euclidian space diffusion). Unlike in the case of SBA-15 mesoporous silica with larger pores [37], the increase in drug weight fraction leads to modifications of the diffusion mechanism, which can be explained by a decrease in drug diffusion and solvent counter diffusion rates as the free mesopore volume decreases. Regarding the ceria- silica mesoporous support MCM-CeO_2, it can be concluded that the doxycycline diffusion process is similar with the pristine MCM-41 silica carrier.

Table II.8. Weibull function parameters describing the experimental doxycycline release data

Parameter	**Doxy dissolution**	**Doxy/CeO_2@MCM-41**	**Doxy)/ MCM-CeO_2**	**Doxy/ MCM-41**	**Doxy2/ MCM-41**
a	0,914	4,357	1,657	1,006	2,105
b	0,679	-0,086	0,194	0,389	0,153
R^2	1	0,9988	0,9986	0,9922	0,9994

In vitro oxytetracycline release experiments were performed in saline phosphate buffer solution at *p*H 5,7 as simulated body fluid [26]. Oxytetracycline, very soluble in water, has low photochemical and chemical stability, especially in basic solutions. From all studied carriers, the antibiotic molecules were completely delivered within a period between 60 to 150 min. (Fig.II.34 and II.35), all release profiles exhibiting a pronounced burst effect, required in the treatment with antibiotics.

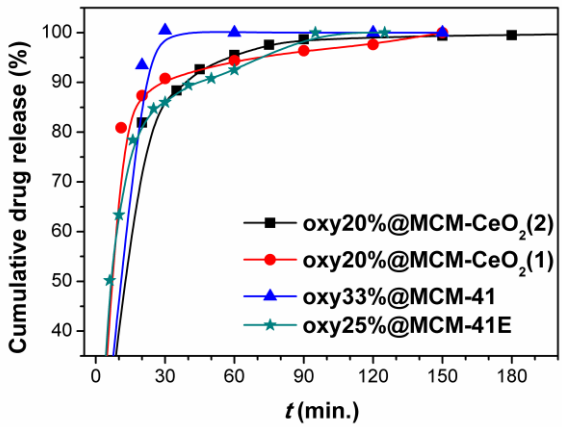

Fig.II.34. Oxytetracycline release profiles from silica-ceria composites compared with MCM-41 silica

The drug delivery from silica-ceria composites was slightly slower than from MCM-41. The higher content of silanol groups in MCM-41E slows down the antibiotic delivery kinetics in comparison with the corresponding calcined MCM-41 carrier. Recently, we reported a similar behavior for doxycycline that had a slower release kinetics from MCM-CeO_2 (1) than MCM-41 silica matrix.

All oxytetracycline-loaded materials containing MCM-41-type silica or aluminosilicate carrier exhibited a delivery profile with a pronounced burst effect, about 60% (wt) of the antibiotic amount being delivered in the first 10 min of the experiment, followed by a gradually release up to 3 h (Fig. II.35). A higher drug amount into the carriers led to slower kinetics (Fig. II.35 B) and a higher aluminum content into the MCM-41-type silica matrix resulted in a lower drug delivery rate (Fig. II.35 A). The cubic pore geometry characteristic for MCM-48 silica didn't favor a gradually drug release, faster kinetics being noticed than for oxytetracycline loaded on MCM-41-type supports (Fig. II.35 B) [41].

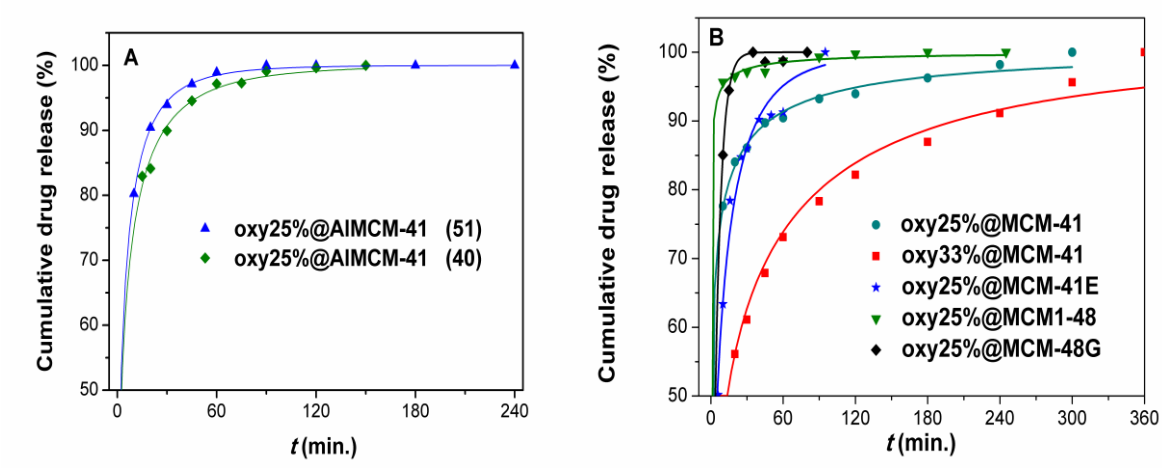

Fig. II.35. The oxytetracycline release profil from aluminosilicate carriers (A) and silica supports (B)

Antimicrobial activity of drug-loaded mesoporous silica-type supports

The antimicrobial activity of doxycycline-loaded MCM-41 or MCM-CeO_2 (1) supports with an antibiotic content of 20% (Table II.7) compared to that of doxycycline cyclate solid powder was evaluated against *Klebsiella ATCC 10031* strain in triplicate.

Tabel II.7. Antimicrobial activity of samples containing doxycycline against *Klebsiella ATCC 10031 strain*

Sample	*Klebsiella pneumoniae ATCC 10031*	*Growth total inhibition zone diameter (mm)*	*Growth partial inhibition zone diameter*
Doxy	++++	35	39
Doxy/MCM-41	++++	35	39
Doxy/MCM-CeO_2(1)	++++	33	38

The bactericidal activity of representative oxytetracycline-loaded materials containing mesoporous silica or aluminosilicate vehicle against five clinical isolates of *Staphylococcus aureus* (SA1-SA5) and the reference ATCC 43300 strains were tested. The oxytetracycline-loaded samples containing MCM-41-type carrier exhibited a significant sensitivity against *S. aureus* ATCC 43300, similar with oxytetracycline alone, while a lower antimicrobial activity for oxytetracycline-loaded MCM-48 sample was found (Table II.11).

Tabel II.11. The bactericidal activity of oxitetracycline-loaded materials

Samples	Microbial strains					
	Staphylococcus aureus					
	SA1	SA2	SA3	SA4	SA5	ATCC 43300
oxy@AlMCM-41 (51)	+++	+++	+++	++	++	++++
oxy@AlMCM-41 (40)	+++	++	+++	++	++	++++
oxy@MCM-41E	+++	+++	+++	+++	+++	++++
oxy@MCM-48	++	++	++	++	++	++
oxytetracycline	+++	++	+++	+++	++	++++

where: + low sensitivity (the measured diameter of the clear area < 10 mm); ++ sensitive (the measured diameter of the clear area between 10–15 mm); +++ distinct sensitivity (the measured diameter of the clear area between 15–25 mm); ++++ significant sensitivity (the measured diameter of the clear area ≥ 30 mm)

The antimicrobial assays demonstrated that oxytetracycline-loaded MCM-41-type carriers inhibited the clinical isolates of *S. aureus* development, the effect being similar or better compared with the antibiotic alone. The most intense inhibitory effect against *S. aureus* 43300 was noticed for

the oxy@MCM-41E material (*D*=39 mm), while for the drug-loaded on commercial AlMCM-41 (40) the average measured inhibition diameter (*D*=31 mm) had the lowest value.

II.5. Composite based on ketoprofen

The influence of mesoporous silica support properties (pore size and geometry, surface functionalization, the drug content) on the ketoprofen delivery kinetics was studied. The ketoprofen-loaded silica samples were then encapsulated into alginate beads and the drug release kinetics from these complex composite carriers into simulated intestinal fluid (pH 7.4) was determined.

For obtaining drug-loaded silica materials, the therapeutic agent was adsorbed into the mesopores of silica-type carriers by incipient wetness impregnation method. In order to study the influence of pore array geometry, two different pristine silica carriers were used, MCM-41 with an ordered 1D hexagonal pore array, presenting a pore diameter of 2.8 nm and a total pore volume of 1 cm^3/g, and MCF exhibiting a higher porosity with a total pore volume up to 3.25 cm^3/g [27,.28] as a result of a continuous three-dimensional disordered pore framework consisting of large spherical pores interconnected by smaller windows [45]. MCF-type silica has the capacity to accommodate a larger amount of guest molecules into its mesopores than MCM-41 or SBA-15. Nevertheless, there are only few studies on MCF silica used as carrier in drug delivery systems, comparing to MCM-41 and SBA-15, especially for poor-soluble therapeutic agents [28, 29]. For the enhancement of acid–base interactions between ketoprofen molecules and silica support, two aminopropyl functionalized silica materials, MCM-APTES and MCF-APTES, with similar content of organic moieties, were also employed. The aminopropyl groups content, determined from thermogravimetric analysis of functionalized silica samples, was 12%(wt) and 12.4%(wt) for MCM-APTES and MCF-APTES, respectively.

The supports and ketoprofen-silica samples were investigated by small- and wide-angle XRD, FTIR spectroscopy and N_2 adsorption-desorption isotherms. The successful functionalization of silica carrier with aminopropyl groups was proved by FTIR spectroscopy, which evidenced the characteristic vibrations of aminopropyl groups.

In all FTIR spectra of ketoprofen-silica composites (Fig.II.37 d-h), one can observe the silica vibrations besides the specific bands of ketoprofen (Table II.12)

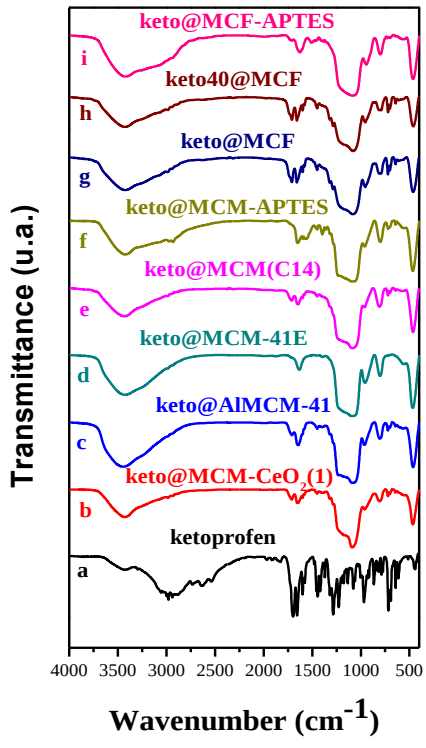

Fig. II.37. Comparision of FTIR spectra of ketoprofen, silica-based carriers and ketoprofen samples

Tabelul II.12. FTIR bands assignment for carriers and ketoprofen samples

FTIR bands assignment	Wavenumber (cm^{-1})
ν_{as}(Si-O-Si)	1085
ν_s(Si-O-Si) /ν_s(Si-O-Al)	800 /804
δ(Al-O)	570
ν(Si-OH)	960
ν(OH)	3433
ν(CO)	1665
ν(COO^-)	1550-1610 $\nu_{C=Oas}$ 1300-1420 $\nu_{C=O}$sim
$\nu_{as}(CH_2)$	2936
$\nu_s(CH_2)$	2855
ν_{NH3+} as și ν_{NH3+} s	3000-3300 m broadband overlapping ν(OH)
δ(NH_3^+)	1575-1600 *i*
δ(NH_3^+)	1300-1500 *i*
$\delta(CH_2)$	1470
νas(CH)	2930
νs(CH)	2855
$\gamma(CH_2)$	695

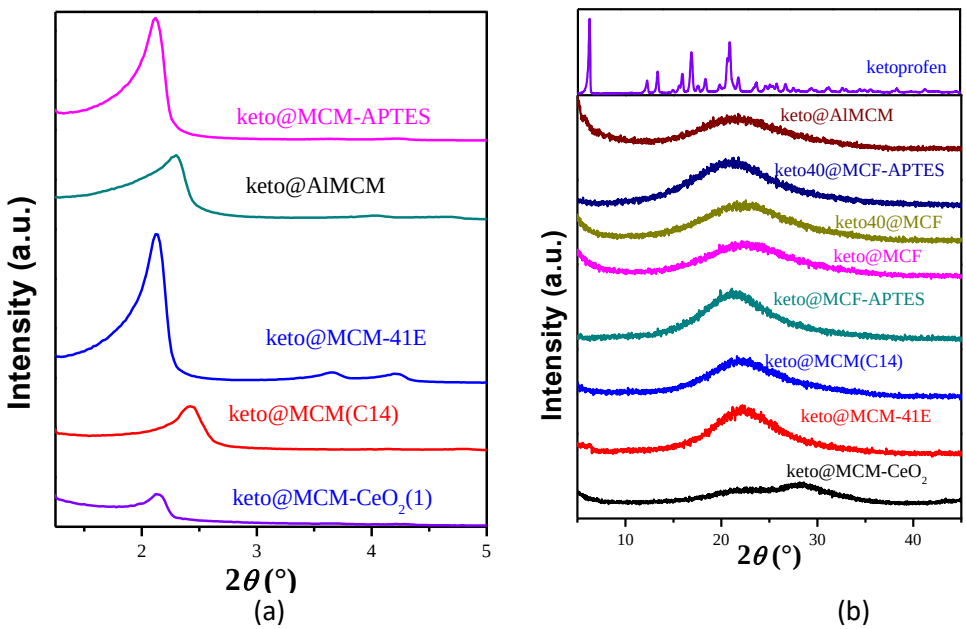

Fig. II.38. Small-angle XRD (a) and wide-angle XRD (b) of ketoprofen samples.

The small-angle XRD patterns of pristine and functionalized MCM-41-type silica materials showed an ordered hexagonal mesophase (Fig. II.38 a and b), while a disordered one being characteristic for MCF materials.

The small-angle XRD of ketoprofen-loaded MCM-41 samples exhibit the intense (100) and less intense (110) and (200) Bragg reflections proving the mesostructure preservation of MCM-41 supports (Fig.II.38 a), after the drug encapsulation. In the wide-angle XRD patterns of the drug-loaded silica samples (Fig. II.38 b), the diffraction peaks of crystalline ketoprofen are not present, indicating that the drug molecules were absorbed into the silica mesopores in amorphous state and no crystalline ketoprofen was form on the silica surface.

The mesoporous silica supports and ketoprofen-loaded silica materials exhibit type IV N_2 adsorption-desorption isotherm (Fig. II.39, II.40 și II.41), characteristic for mesoporus materials, completely reversible for MCM-41-type samples and with a large H1 hysteresis loop for MCF-based materials because of sharp capillary condensation in the 0,65-0,9 relative pressure range. The adsorption-desorption isotherms of ketoprofen-loaded silica materials proved the adsorption of drug molecules into the support mesopores, their total porosity being lower than that of the corresponding carrier (Fig.II.39 A and II.40 A). The textural parameters (specific surface area, S_{BET}, total pore volume, V_{pore}, and average pore diameter, d) determined from N_2 adsorption-desorption isotherms for the ketoprofen-loaded silica samples compared with silica carriers are shown in Tabel II.13.

Tabelul II.13. The textural parameters for carriers and ketoprofen-loaded silica samples

Carrier	S_{BET} (m^2/g)	V_p (cm^3/g)	d_{BJH} (nm)	Composite	S_{BET} (m^2/g)	V_p (cm^3/g)	d_{BJH} (nm)
MCM-CeO_2 (1)	683	0.67	2.66	keto@MCM-CeO_2(1)	235	0.08	2.00
MCM-41E	818	0.78	2.82	keto@MCM-41E	536	0.51	2.25
MCM(C14)	654	0.80	2.13	keto@MCM(C14)	161	0.09	1.76
MCM-APTES	585	0.51	2.39	keto@MCM-APTES	279	0.19	1.76
MCF	876	2.29	16.68	keto@MCF	377	1.49	16.09
				keto40@MCF	183	0.87	13.94
MCF-APTES	518	1.98	9.02	keto@MCF-APTES	377	1.75	9.03
AlMCM-41	729	0.66	2.38	keto@AlMCM-41	580	0.34	1.99

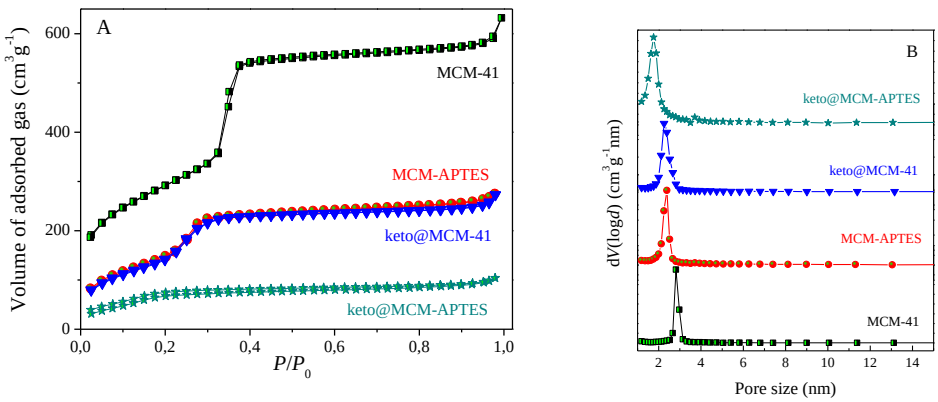

Fig.II.39. N_2 adsorption-desorption isotherms of MCM-41-type supports and ketoprofen-loaded samples containing MCM-41-type carriers (A) and their pore size distribution curves (B)

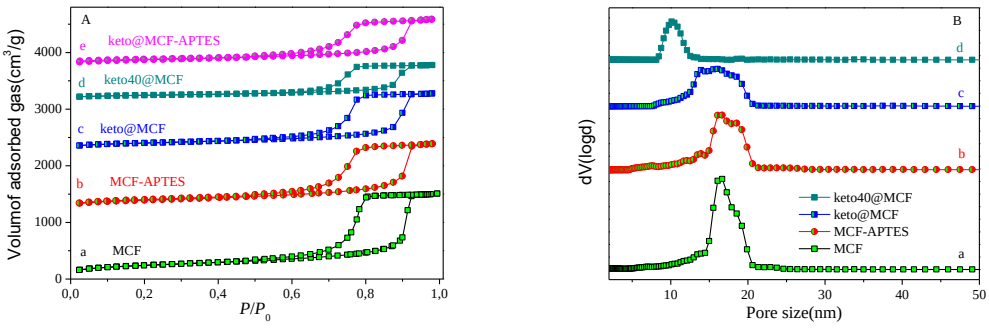

Fig. II.40. N_2 adsorption-desorption isotherms of MCF-type supports and ketoprofen-loaded samples containing MCM-41-type carriers (A) and their pore size distribution curves computed with DFT model (B)

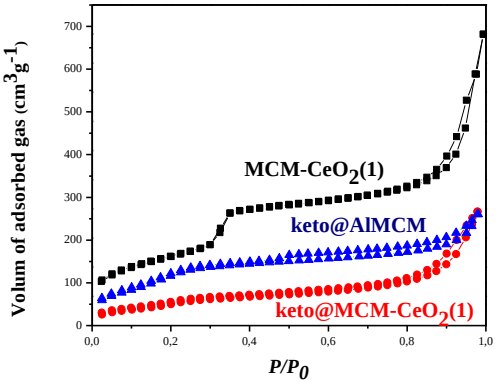

Fig. II.41 N_2 adsorption-desorption isotherms for ketoprofen-loaded samples

Both 3-aminopropyl functionalized silica supports present lower specific surface area and average pore diameter than the pristine silica materials from which they were obtained meaning that the organic moieties are linked on the internal silica pore walls surface (Table II.13). Although the functionalization with aminopropyl groups of silica materials caused a slight decrease of textural parameter values, all supports exhibited large porosity required for their application as vehicles for biologically active molecules. The samples containing ketoprofen presented some porosity, which diminished with the increase of therapeutic agent content. The pore size distribution curves and average pore diameter were calculated using Barrett-Joyner-Halenda (BJH) method for MCM-41-type samples from the desorption branch of isotherms (Fig. II.39B) and DFT model for MCF-type materials (Fig. 40B). One can observe a decrease of the average pore diameter of drug-loaded materials compared with that of the corresponding carrier (Fig.II.40 and II.41) because of either the ketoprofen adsorption into carrier mesopores or the interactions between drug molecules and silica-type support (Table II.13).

The determination of ketoprofen *in vitro* release profile from mesoporous silica carriers (Fig. II. 42.A) was performed in simulated intestinal fluid, saline PBS, pH 7.4, at 37°C, under constant magnetic stirring, using a dialysis membrane. The ketoprofen dissolution test was carried out in the same conditions using also a dialysis bag. The drug delivery profiles are plotted in figure II.42, as drug cumulative release with respect to the time.

The therapeutic agent exhibited fast release kinetics from pristine silica carriers in the first hour of experiment, even faster than its dissolution, in the case of keto@MCF, followed by a sustained release, more pronounced in the case of aminopropyl-functionalized silica supports due to acid-base interactions (Fig.II.45). The fast first stage of ketoprofen release from silica supports, especially for pristine ones, could be explained by the diffusion of drug molecules, which are more soluble in basic medium in amorphous state than as crystals. The second stage of ketoprofen release is slower when drug molecules, which are stronger linked on silica surface through acid-base interactions, are gradually delivery in simulated intestinal fluid. One can observe a lower drug release rate at high amount of therapeutic agent adsorbed into the mesopores of pristine MCF silica.

The ketoprofen experimental release data were fitted with good correlation coefficients, $R^2_w>0.95$, using the Weibull model, a two parameters exponential function based on the theory of percolation in both Euclidian and fractal space (Fig.II.42A), which is highly applied for the drug dissolution from different matrices. Table II.14 lists the obtained *a* and *b* parameters, as well as the correlation coefficients, R^2_W, for the Weibull model. One can notice that the *b* parameter values correspond to a drug Fick's diffusion in fractal space, being lower than 0,69 [31].

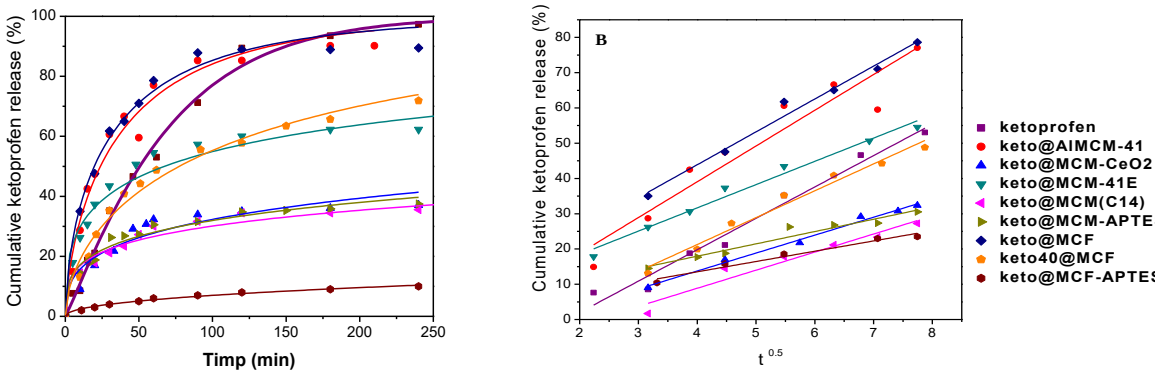

Fig. II.42. Ketoprofen release profiles from pristine and functionalized silica-type carriers fitted with Weibull function (A) and Higuchi model (B)

To evaluate the ketoprofen release rate in the burst stage, the drug delivery experimental data from the first hour of the experiments were fitted with the Higuchi`s model: $m(t)/m(\infty)=k_H t^{1/2}$, were k_H is the rate constant (Fig.II.42B) [36]. The k_H values and the correlation coefficients, R^2_H, obtained for all ketoprofen-loaded silica materials are listed in Table II.14. The slowest ketoprofen delivery kinetics for the burst stage of drug release was obtained in the case of MCF-APTES carrier, followed by MCM-APTES support due to the acid-base interactions between amino moieties linked on carrier mesopores surface and ketoprofen carboxyl groups. In the case of pristine silica support, lower delivery rate of ketoprofen was noticed for MCM-41E than for MCF, which could be explained by either a smaller average pore diameter and an ordered pore array or a higher content of silanol groups as the support was not calcined, unlike MCF carrier.

Table II.14 WEIBULL and HIGUCHI parameters obtained by fitting the experimental data of drug release from silica-type carriers

Samples	Weibull model			Higuchi's function	
	a	*b*	R^2_W	k_H	R^2_H
ketoprofen	0.009	1.111	0.994	8.698	0.975
keto@MCM-41E	0.157	0.351	0.951	6.594	0.979
keto@MCM-APTES	0.076	0.284	0.955	3.498	0.936
keto@MCF	0.1072	0.626	0.983	9.316	0.979
keto40@MCF	0.0543	0.585	0.981	7.621	0.973
keto@MCF-APTES	0.0082	0.473	0.972	2.919	0.956

To prepare drug-silica-alginate beads, keto@MCM-41E and keto@MCF-APTES were chosen, both samples having 20%(wt) drug content. The chosen drug-loaded silica samples presented the lowest total cumulative release and the slowest release kinetics among pristine silica and functionalized silica carriers, respectively. The obtained ketoprofen-silica-alginate, denoted keto@MCM-alg and keto@MCF-APTES-alg, were investigated by SEM-EDX and thermal analysis. The content of ketoprofen, which remained in the silica-alginate beads, was determined by measuring the drug amount delivered in calcium chloride solution during the beads formation using UV-vis spectroscopy. About a third part of ketoprofen was released from either MCM-41 support or MCF-APTES material in calcium chloride aqueous solution, resulting a content of drug in beads of 2,2%(wt).

The SEM investigation of ketoprofen-silica-alginate composites revealed the formation of spherical beads with a diameter in the range of 0.8-1.2 mm (Fig. II.48). On the beads surface one can observe the formation of sodium chloride crystals, though the beads were intensively washed with ultrapure water (Fig. II.48). The EDX analysis coupled with SEM investigation showed that silica particles are inside the alginate beads, calcium ions penetrate the polymer network and on the alginate surface there are still sodium chloride crystals.

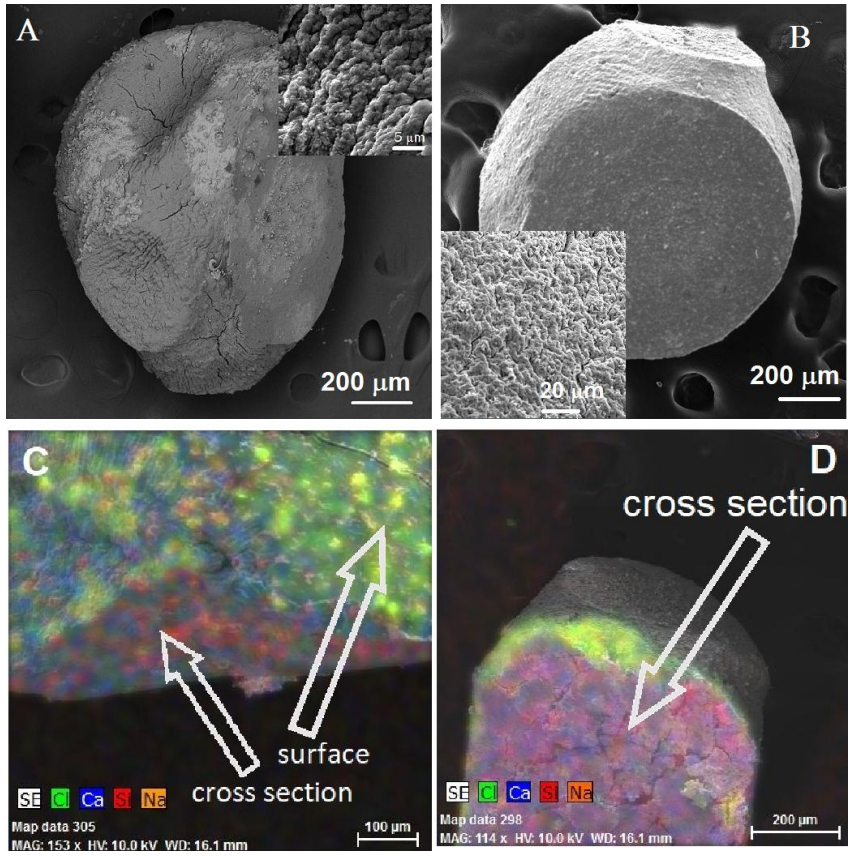

Fig. II.49. SEM images of: A) keto@MCM-alg (inset its surface), B) keto@MCF-APTES-alg (inset its surface), and EDX elemental mapping of: C) keto@MCM-alg and D) keto@MCF-APTES-alg beads

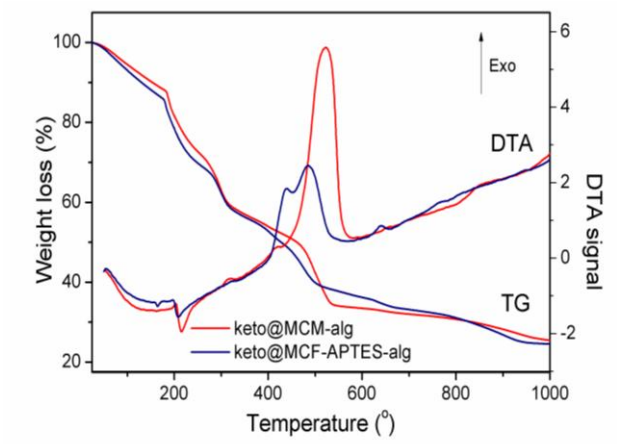

Fig. II.53. DTA-TG analysis of ketoprofen-silica-alginate beads

The DTA-TG analysis of ketoprofen-silica-alginate beads showed a thermal decomposition in several steps (Fig. II.53). In the temperature range of 20º-170ºC, both-types of beads lose water from alginate hydrogel and silica mesopores. At 170ºC, alginate begins to decompose, and the process continues up to 600ºC [37]. On the DTA curves, two strong exothermic effects can be noticed in the 400º-580ºC temperature range. The residue mass for keto@MCM-alg and keto@MCF-APTES-alg was 25.6% and 24.5%, respectively, which consisted of 15.9% (wt) silica and 9.7% (wt) compounds containing calcium and sodium ions for the first sample and 14% and 10.5% for the second one. Ketoprofen melts at 97ºC, it is stable up to around 170ºC and totally decomposes at 376ºC [38, 39]. Because in the silica-alginate beads the content of ketoprofen is low, its thermal decomposition, in the temperature range of 170º-376ºC, is difficult to notice, being overlapped with that of alginate, which is in a higher amount in the samples.

The experiments of ketoprofen delivery from silica-alginate beads, carried out in the same conditions as for drug-loaded silica samples, showed slower kinetics in comparison with the

ketoprofen-loaded silica carriers. The drug release experimental data were also fitted with the Weibull function (Fig. 9) with the correlation coefficient of 0.977 and 0.954 for keto@MCM-alg sample and keto@MCF-APTES-alg beads, respectively. As in the case of the ketoprofen delivery from silica-type carriers, the exponential *b* parameter of the Weibull function has values of 0,514 and 0,321 for keto@MCM-alg and keto@MCF-APTES-alg, respectively, corresponding to a Fickian diffusion of the therapeutic agent. For both type of alginate beads, the pre-exponential parameter *a* of the Weibull function has the same value of 0.0103, because it depends on the surface through which ketoprofen diffusion occurs. This can be explained by the high contribution of alginate which is in large and similar amount in both type of ketoprofen-loaded silica-alginate beads. One can notice a higher release rate of ketoprofen from MCM-alg beads than from MCF-APTES-alg, the similar trend being also observed for the corresponding ketoprofen-loaded silica samples.

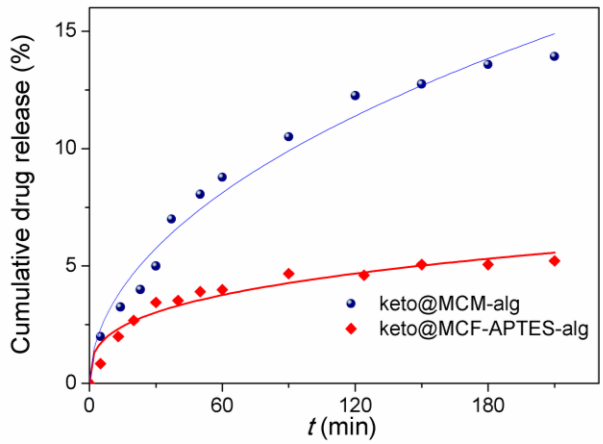

Fig. II.54 Ketoprofen release profiles from silica-alginate beads fitted with the Weibull function

II.6. Composites based on doxorubicin

The last objective of this thesis was the encapsulation of doxorubicin, a cytostatic agent used in the treatment of several forms of cancer, in magnetite-aluminosilicate-type composite materials, and studies on the drug release profiles in the biological fluid that simulates the tumor cell environment. For doxorubicin, Fe_3O_4@AlMCM-41, Fe_3O_4@AlSBA-15, Fe_3O_4@AlMCM-41-PEG and SBA-15 fuctionalized with folate groups as carriers were chosen. Doxorubicin was adsorbed into carrier mesopores by the same method, incipient wetness impregnation.

For all doxorubicin-loaded magnetic mesoporous matrix, FTIR spectra exhibit the vibrations corresponding to the main functional groups of doxorubicin, besides the bands characteristic for magnetic mesoporous carrier (Fig. II.55).

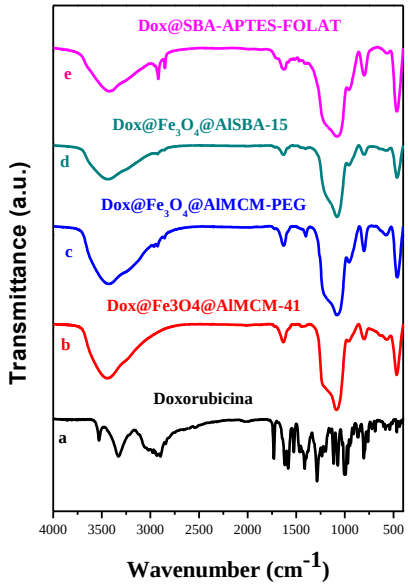

Fig. II.55. FTIR spectra of doxorubicin and doxorubicin-loaded magnetic carrier

Wide-angle XRD (Fig II.55A) patterns for doxorubicin-loaded materials exhibit only the Bragg reflections characteristic of crystalline magnetite phase along with the large diffraction peak in the range of 20-40° 2θ, characteristic for amorphous silica. The DOX@Fe_3O_4-AlMCM-PEG material exhibited a hexagonal pore framework with mesochannels preservation, characteristic of MCM-41 materials as small-angle proved (Figure II.55B).

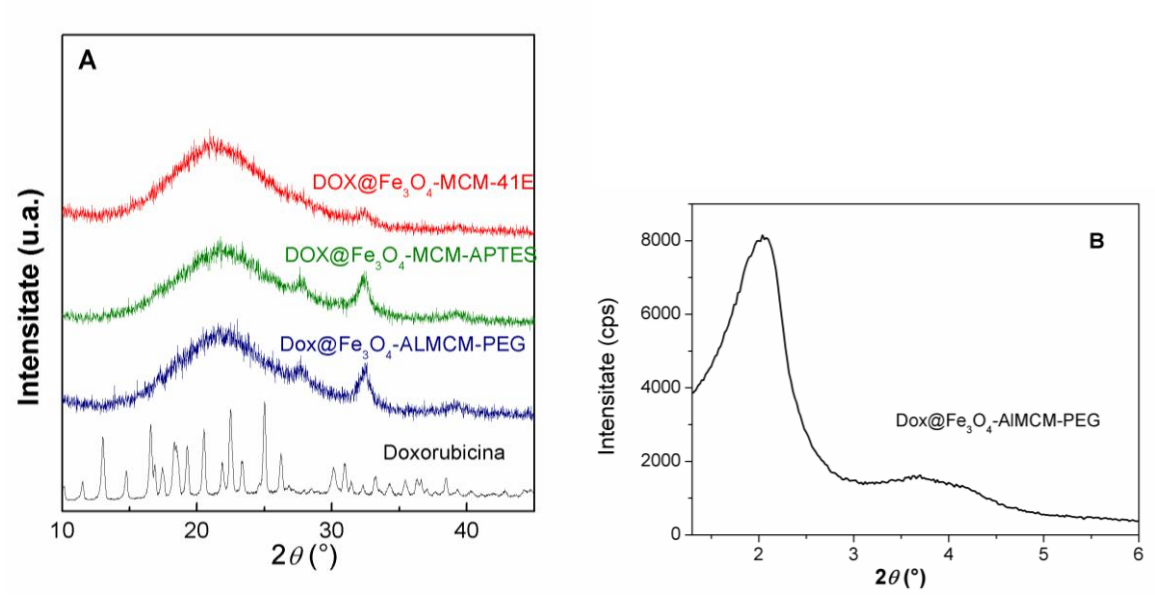

Fig. II.55. Wide-angle XRD for doxorubicin-loaded samples (A) and small-angle of DOX@Fe_3O_4-AlMCM-41-PEG (B).

N_2 adsorption-desorption isotherms, recorded at 77K showed that the porosity of doxorubicin-loaded materials is lower than that of the corresponding carrier (Fig. II.56) due to the presence of therapeutic agent molecules into the carrier mesopores. Table II.15 lists the textural parameters of doxorubicin-loaded samples and those of the correspondig vehicles. The presence of aluminum into the silica matrix, which leads to Lewis acidity and thus enhances the interactions between the cytostatic agent and carrier, evidenced by the decrease in the average pore size of doxorubicin-loaded materials compared to coresponding carrier (Table II.15).

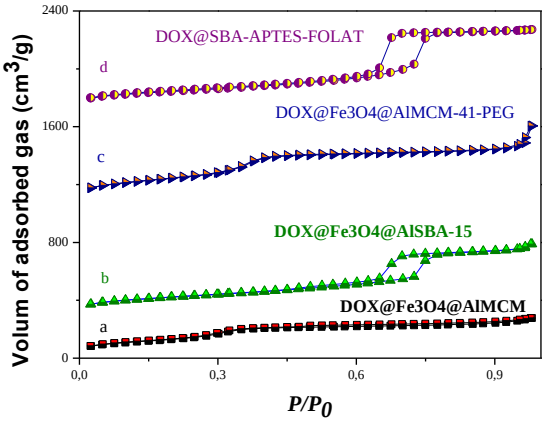

Fig. II.56. N_2 adsorption-desorption isotherms for doxorubicin composites

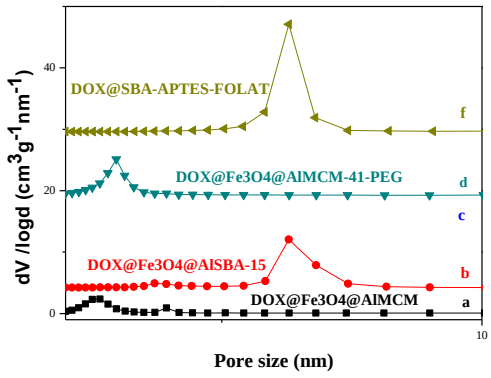

Fig. II.57. Pore size distribution for doxorubicin composites

Tabelul II.15. The textural parameters of therapeutic agent-loaded materials in comparision with coresponding magnetic mesoporous matrix

Samples	Doxorubicin-loaded materials			Carrier			
	S_{BET} (m_2/g)	V_{pori} (cm^3/g)	d_{BJH} (nm)	S_{BET} (m_2/g)	V_{pori} (cm^3/g)	d_{BJH} (nm)	M_s (emu/g)
DOX@ Fe_3O_4@AlMCM	497	0.46	2.51	609	0.57	2.66	6.42
DOX@ Fe_3O_4@AlMCM-PEG	680	0.61 d<10 nm	2.97	852	0.90	2.98	ND*
DOX@Fe_3O_4@AlSBA-15	469	0.70 d<10 nm	6.29	829	0.88 d<10nm	6.81	4.21
DOX@SBA-APTES-FOLAT	447	0.90	6.29	472	0.906	6.28	ND*

ND* = indefinite

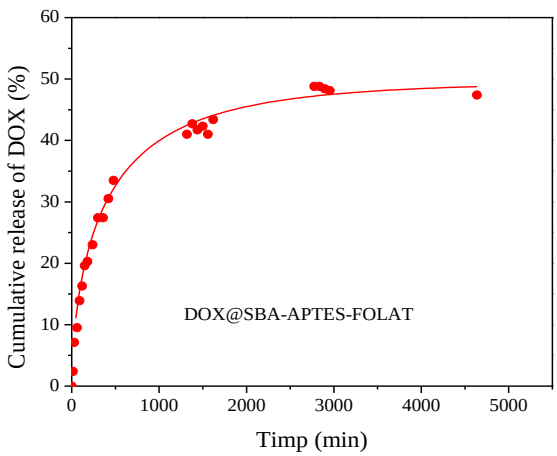

Fig. II.58. Doxorubicin release profile from SBA-APTES-FOLATE carrier

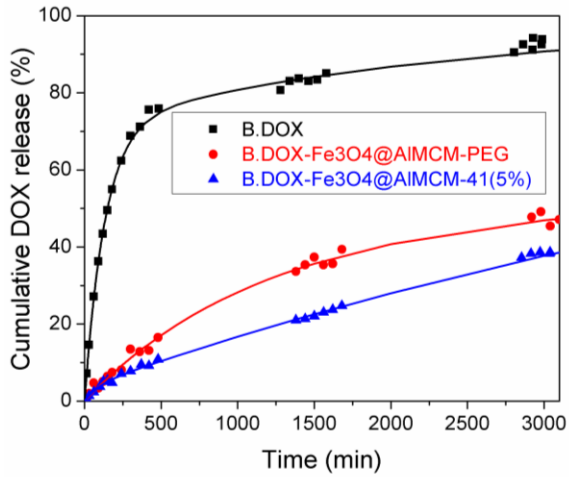

Fig. II.59. Doxorubicin release profile from Fe_3O_4@AlMCM-41 and Fe_3O_4@AlMCM-PEG in comparisin with doxorubicin dissolution

One can observe that doxorubicin release from Fe_3O_4@AlMCM-41 (Fig. II.59) was slower than from Fe_3O_4@MCM-41, which can be explained by acid-base interactions between the acidic aluminosilicate surface and cytostatic agent, which has base nature. This is beneficial, leading to a decrease in its toxicity for feathy tissues, improving the treatment efficiency.

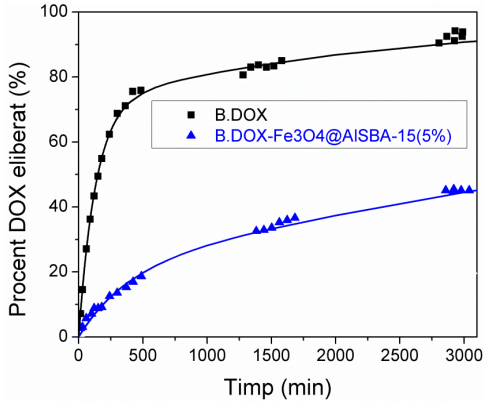

Fig. II.60. Release profile of DOX from Fe_3O_4@AlSBA-15

Due to a good DOX release kinetics from Fe_3O_4@AlMCM-41 carrier, a similar material functionalized with polyethylene glycol (PEG) moieties was synthesized, characterized and applied as vehicle for doxorubicin. The sample prepared by doxorubicin adsorption into mesopores of this carrier, in the same amount as in DOX-Fe_3O_4@AlMCM-41 material, was denoted DOX-Fe_3O_4@AlMCM-PEG, and its drug release profile is shown in figure II.59 in comparison with that of DOX@Fe_3O_4@AlMCM-41. A slight increase in the release rate of the therapeutic agent can be observed, probably because of polymer linked on aluminosilicate surface. The Fe_3O_4@AlMCM-41-PEG material can be used as vehicle for targeted tumoral tissue through passive accumulation due to the presence of PEG moieties. One can notice that for DOX-Fe_3O_4@AlMCM-PEG sample, the total cumulative drug release is higher than that for DOX-Fe_3O_4@AlMCM-41 material.

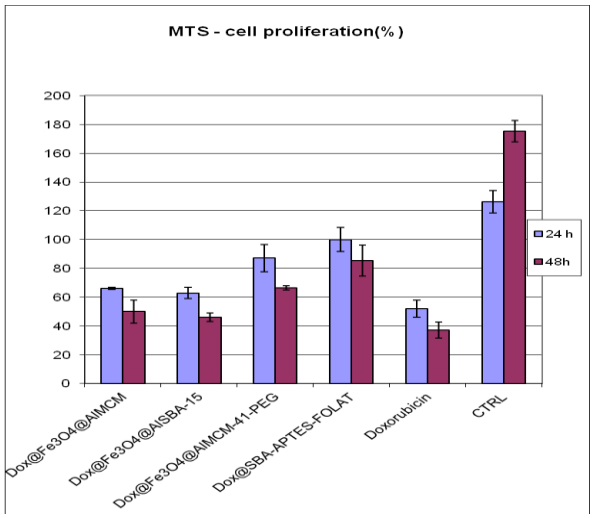

Fig. II.62 Toxicity assays of doxorubicin and doxorubicin-loaded magnetite-aluminosilicat carriers

The toxicity of doxorubicin-loaded was assesed on healthy human lymphocytes line by using the CellTiter 96R AQ_{ueous} One Solution Cell Proliferation Assay (MTS, Promega).[46] The cytotoxicity was evaluated using a standardized assay based on colored formazan production in metabolically active cells. After 24 h and 48 h exposure to 5 μg mL^{-1} DOX or equivalent cytostatic agent in drug-loaded samples. The doxorubicin encapsulation into mesopores of magnetite-aluminosilicate or SBA-APTES-FOLATE carriers determined an increase of cell viability in comparison with the drug aqueous solution, in the same concentration in cellular medium.

Conclusions

In this PhD thesis, several inorganic mesostructured materials were synthesized and characterized: silica-ceria composites, pristine and aminopropyl functionalized silica materials,

aluminosilicate, magnetite coated with AlMCM-41 and AlSBA -15-type aluminosilicate.

Silica-ceria mesoporous composites were obtained by two methods. The first approach consists in obtaining ceria nanoparticles by the hydrothermal method in the presence of CTAB as a stabilizer, foolowed by their coating with MCM-41-type silica. The second method consists in obtaining the composites in a single step, in basic medium, in the presence of CTAB as a structuring agent, through sol-gel technique assisted by a hydrothermal treatment that led to the formation of a mesophase with an ordered pore array, as well as the crystallization of ceria phase with fluorite structure and cubic symmetry. By the second method, two composites with different ceria content, MCM-CeO_2 (1) with 10% (mol) ceria and MCM-CeO_2 (2) with 20% (mol) ceria were synthesized and characterized. The removal of surfactant molecules for all silica-ceria composites was performed by calcination at 550 °C/5h. In the case of second method, the TEM investigation evidenced the formation of the mesostructured silica coated with ceria nanoparticles with a diameter of about 5 nm.

For the first time, ceria-silica composites with an ordered hexagonal pore framework were used as carriers in drug delivery systems, their behavior being compared to that of MCM-41 and MCF silica and AlMCM-41-type aluminosilicates.

Three mesoporous composite materials with superparamagnetic behavior were synthesized for the development of targeted drug delivery systems. The composite materials were obtained by coating Fe_3O_4 nanoparticles priviously obtained through the decomposition of Fe(III) tris-acetylacetonate, with AlMCM-41 and AlSBA-15-type aluminosilicates. For passive accumulation in tumor tissue, the magnetite nanoparticles were coated with AlMCM-41 functionalized with polyethylene glycol moieties. The behavior of SBA-APTES-material as carrier for doxorubicin was also studied.

The carriers and drug–loaded samples were characterized by various techniques: wide- and small-angles XRD, FTIR spectroscopy, N_2 adsorption-desorption isotherms, SEM and TEM etc.

Two types of mesoporous silica were functionalized with aminopropyl groups by post-synthesis method, which were further employed as carriers for ketoprofen. These functionalized supports led to a slower ketoprofen delivery kinetics than in the case of pristine silica due to acid-base interactions between drug molecules and carrier, which are stronger than van der Waals and hydrogen bonds formed between pristine silica and ketoprofen.

Another objective of the PhD thesis was the development of antibiotic delivery systems containing MCM-41-type supports: silica, silica-ceria composites and aluminosilicate. Doxycyline and oxytetracycline molecules from the tetracycline class, were chosen, both being very soluble in water. Their adsorption into carrier mesopores was carried out by incipient wetness impregnation method. Wide-angle XRD analysis demonstrated that antibiotic molecules were adsorbed onto carrier mesopores in amourphous state and N_2 adsorption-desorption isotherms of antibiotic-loaded materials evidenced a decrease in their porosity and average pore diameter values in comparison with that of the corresponding support. The evaluation of antimicrobial activity demonstrated that the adsorption of antibiotics into carrier mesopores did not influence their bactericidal activity.

The introduction of aluminum atoms into the silica framework determine an increase of Lewis acidity and a decrease of antibiotic release rate. A higher amount of antibiotic into MCM-41 carrier mesopores slowed down the drug delivery kinetics. The experimental data of doxycyclin and oxytetracycline release profiles were fitted with Weibull model, a two parameters exponential function. For both antibiotics, based on b parameter values of Weibull function, the drug transport mechanism was a fickian diffusion.

Also, ketoprofen-based composites containing MCM-41 and MCF pristine and aminopropyl functionalized silica, aluminosilicate and MCM-CeO_2 (1) as carriers were synthesized and characterized. The slowest kinetics of ketoprofen release from mesoporous silica-type carrier in simulated intestinal fluid, phosphate buffer saline, *p*H 7.4, was obtained for the keto@MCF-APTES sample.

The keto@MCM-41 and keto@MCF-APTES samples with 20% drug content were selected to obtain more complex drug delivery systems by encapsulating the ketoprofen-silica composite in alginate beads by ionotropic gelation technique. The SEM analysis evidenced the formation of alginate beads comprising ketoprofen-loaded mesoporous silica particles, as well as the presence of

calcium ions inside the polymer. Ketoprofen release from silica-alginate beads was slower than from functionalized silica demonstrating that the use of alginate is beneficial. Alginate is insoluble in acidic medium, so ketoprofen can reach the intestinal tract where it is released from silica-alginate beads, therefore the side-effects in stomach are reduced.

The final objective of PhD thesis was the encapsulation of doxorubicin, a cytostatic agent used in the treatment of many forms of cancer, in inorganic magnetite-aluminosilicate composites. The doxorubicin release profiles were determined in the biological fluid simulating the tumor cell environment, the phosphate buffer solution, *p*H 5.7. A high efficiency of cytostatic agent encapsulation was observed, its desorption from the magnetic carriers being very slow. The presence of aluminum in the silica matrix has led to better drug encapsulation due to strong Lewis acid-base interactions between doxorubicin posively charged and magnetite-aluminosilicate-type carrier. The slowest drug release kinetics was obtained for DOX-Fe_3O_4@AlMCM-41 sample.

The entrapment of doxorubicin into magnetite-aluminosilicate-type or SBA-APTES-FOLATE carriers led to an enhanced cell viability in comparison with that for the cytostatic agent aqueous solution, in the same concentration in the cellular medium.

Original contribution

The aim of this PhD thesis was the development of drug delivery systems containing different active pharmaceutical ingredeints and various types of pure and functionalized mesoporous silica, silica-ceria and magnetite-aluminosilicate composites as carriers. For the first time, silica-ceria MCM-41-type composites were tested as supports in drug delivery systems by combining ceria antioxidant properties with the remarkable loading capacity of mesostructured silica. In this work, doxycycline delivery systems containing silica-ceria mesoporous composite carriers were obtained and compared with doxyxline-loaded MCM-41 silica. Also, oxytetracycline delivery systems were prepared and characterized containing MCM-41 silica, silica-ceria composites with different ceria content (10% and 20% mol), AlMCM-41 and MCM-48 carriers. The influence of ceria nanoparticles or aluminum atoms in MCM-41 silica network on the *in vitro* release profiles was studied. The novelty of this thesis consists also in the development of more complex systems obtained by encapsulation of ketoprofen-silica materials in alginate beads for gastric protection because ketoprofen leads to gastric ulceration as side-effect, the developed systems being able to reach the intestinal tract. Another active pharmaceutical ingredient used for the design of targeted drug delivery systems was doxorubicin. In this case, the vehicles employed for the doxorubicin encapsulation were magnetite coated with mesoporous aluminosilicate, the presence of aluminum in the silica network favoring a more efficient entrapment of the cytostatic agent due to strong acid-base interactions between the support and drug molecules.

Perspectives

- ✓ Biocompatibility and toxicity evaluation of mezoporous silica-ceria carriers and their antioxidant properties.
- ✓ Development of targeted drug delivery systems based on other cytostatic agents using functionalised magnetite-aluminosilicate composite as vehicles.
- ✓ Toxycity assays on doxorubicin-targeted delivery systems on several tumoral cells line.

Articles published in ISI journals

- D. Berger, S. Nastase, R.A. Mitran, M. Petrescu, E. Vasile, C. Matei, T. Negreanu-Pirjol, *Mesostructured silica and aluminosilicate carriers for oxytetracycline delivery systems,* International Journal of Pharmaceutics 510 (2016) 524-531 (FI=3.649)
- M. Petrescu, R.A. Mitran, C. Matei, D. Berger, *Mesoporous silica-ceria composites as carriers for drug delivery systems,* Revue Roumaine de Chimie, 2016, 61(6-7), 557-563 (FI=0.246)
- M. Petrescu, R. A. Mitran, A.M. Luchian, C. Matei, D. Berger, *Mesoporous ceria-silica composites as carriers for doxycycline*, UPB Sci Bull., Series B, 77, Iss 3 (2015)13-24 (ISSN: 1454-2331) - without IF
- M. Petrescu, R.A. Mitran, C. Matei, M. Radulescu, D. Berger, *Silica-Alginate Composites for Intestinal Ketoprofen Delivery,* Revista de Chimie 12 (2018) – in press

Conferences

- M. Petrescu, R.A. Mitran, C. Matei, D. Berger, *Mesoporous silica-ceria composites as carriers for drug delivery systems,* Zilele Universităţii "Alexandru Ioan Cuza" din Iaşi, Iași, 2015
- M. Petrescu, R.A. Mitran, C. Matei, D. Berger, *Studies on mesoporous silica as carriers for ketoprofen,* PRIOCHEM XII – 2016, secțiunea a 3-a – Materiale multifuncționale și nanocompozite

II.8. References

[1] M. Vallet-Regí, F. Balas, and D. Arcos, *Mesoporous materials for drug delivery,* Angew. Chemie - Int. Ed., 46(40), **2007**, 7548–7558,

[2] R. C. S. Azevedo, R. G. Sousa, W. A. A. Macedo, E. M. B. Sousa, *Combining mesoporous silica–magnetite and thermally-sensitive polymers for applications in hyperthermia,* J Sol-Gel Sci Technol, **72** (2), **2014**, 208-218

[3] R.-A. Mitran, D. Berger, L. Băjenaru, S. Năstase, C. Andronescu, C. Matei, *Azobenzene functionalized mesoporous AlMCM-41-type support for drug release applications,* cent.eur.j.chem., **12** (7), **2014**, 788-795

[4] R. Liang, M. Wei, D. G. Evans, X. Duan, *Inorganic nanomaterials for bioimagin, targeted drug delivery and therapeutics*, Chemical Communications, 50, **2014,** 14071-14081

[5] R.-A. Mitran, S. Nastase, C. Matei, D. Berger, *Tailoring the dissolution rate enhancement of aminoglutethimide by functionalization of MCM-41 silica: a hydrogen bonding propensity approach,* RSC Advances, **5** (4), **2015,** 2592-2601

[6] D. Schubert, R. Dargusch, J. Raitano, S.W. Chan, *Cerium and yttrium oxide nanoparticles are neuroprotective,* Biochem. Biophys. Res. Com, 42, **2006**, 86–91,

[7] I. Celardo, J.Z. Pedersen, E. Traversa, L. Ghibelli, Nanoscale, 3, **2011,** 1411-1420

[8] L. Kong, X. Cai, X. H. Zhou, L. L. Wong, A. S. Karakoti, S. Seal, J. F. McGinnis, *Nanoceria extend photoreceptor cell lifespan in tubby mice by modulation of apoptosis/survival signaling pathways,* Neurobiol Dis., 42, **2011**, 514-523,

[9] J. L. Niu, A. Azfer, L. M. Rogers, X. H. Wang, P. E. Kolattukudy, *Cardioprotective effects of cerium oxide nanoparticles in a transgenic murine model of cardiomyopathy,* Cardiovasc. Res., 73, **2007,** 549–559

[10] C. K. Kim, T. Kim, I.-Y. Choi, M. Soh, Dg Kim, Y.-Ju Kim, H. Jang, H-S. Yang, J. Y. Kim, H.K. Park, S. P. Park, S. Park, T. Yu. B.-W. Yoon, S.-H. Lee, T. wan Hyeon, *Ceria nanoparticles that can protect against ischemic stroke,* Angew. Chem. Int. Ed., 51, **2012**, 11039-11043,

[11] A. Hayat, D. Andreescu, G. Bulbul, S. Andreescu, *Redox reactivity of cerium oxide nanoparticles against dopamine,* J. Coll. Inter. Sci, 418, **2014**, 240–245

[12] H. Iwasaki, H. Inoue, Y. Mitsuk, A. Badran, S. Ikegaya, T. Ueda, *Doxycycline induces apoptosis by way of caspase-3 activation with inhibition of matrix metalloproteinase in human T-lymphoblastic leukemia CCRF-CEM cells*, Journal of Laboratory and Clinical Medicine, 140 (6), **2002**, 382-386

[13] W. C. M. Duivenvoorden, S. V. Popović, Š. Lhoták, E. Seidlitz, H. W. Hirte, R. G. Tozer, G. Singh, *Doxycycline Decreases Tumor Burden in a Bone Metastasis Model of Human Breast Cancer, Cancer Research*, 62 (6), **2002**, 1588-1591

[14] N. Holmes, P. Charles, *Safety and efficacy review of doxycycline*, Clinical Medicine: Therapeutics, 1, **2009,** 471–482

[15] E.C. Perreira-Maia, P.P. Silva, W.B. De Almeida, H.F. Dos Santos, B.L. Marcial, R. Ruggeiro, W. Guerra, *Tetracyclines and glycylclines: An overview*, Quimica Nova, 33, **2010**, 700-706,

[16] K. Chatterjee, J. Zhang, N.Honbo, J. S. Karliner, *Doxorubicin Cardiomyopathy*, Cardiology, 115, **2010**, 155-162

[17] F. Maseras, K.Morokuma, *IMOMM: A new integrated* ab initio + *molecular mechanics geometry optimization scheme of equilibrium structures and transition states* , J.Comput.Chem, 16 (9), **1995**, 1170-1179

[18] J. R. Shoemaker, L. W. Burggraf, M. S. Gordon, *An ab initio cluster study of the structure of the Si(001) surface*, J. Chem. Phys. A, 112, **2000,** 2994

[19] J.R.Shoemaker, L.W.Burggraf, M.S.Gordon, J. Phys. Chem. A, 103, **1999**, 3245-51

[20] C. H. Choi, M. S. Gordon, J. Am. Chem. Soc, 121, **1999**, 11311-7

[21] Y. Jung, C. H. Choi, M. S. Gordon, J. Chem. Phys. B, 105(18), **2001**, 4039-44

[22] C. H. Choi, D.-J. Liu, J. W. Evans, M. S. Gordon, *Passive and Active Oxidation of Si(100) by Atomic Oxygen: A Theoretical Study of Possible Reaction Mechanisms*, J. Am. Chem. Soc, 124 (29), **2002**, 8730-8740

[23] Y. Jung, Y. Akinaga, K. D. Jordan, M. S. Gordon, Theoret. Chem. Acc, 109, **2003**, 268-73

[24] C. H. Choi, M. S. Gordon, J. Am. Chem. Soc, 124, **2002,** 6162

[25] Jan H. Jensen, *Molecular Modeling Basics*, CRC Press, Taylor and Francis Group, ISBN 978-1-4200-7527-4, **2010**, 25-76

[26] M. R. C. Marques, R. Loebenberg, M. Almukainzi, *Simulated Biological Fluids with Possible Application in Dissolution Testing*, Dissolution Technologies, 18(3), **2011**, 15-28,

[27] Wan, Y., Zhao, D. *Chem. Rev.* 107, **2007**, 2821

[28] Jia. L. J., Shen. J. Y., Li. Z.Y., Zhang. D.R., Zhang. Q., Lin. G.P., Zheng. D.D., Tian. X.N., *In vitro and in vivo evaluation of paclitaxel-loaded mesoporous silica nanoparticles with three pore sizes*, Int. J. Pharm, 445, **2013**, 12–19

[29] Martínez. L., Villalobos. R., Sánchez. M., Cruz. J., Ganem. A., Melgoza. L.M., *Monte Carlo simulations for the study of drug release from cylindrical matrix systems with an inert nucleus*, Int. J. Pharm. 369, **2009**, 38–46.

[30] Nastase. S., Bajenaru. L., Matei. C., Mitran. R.A., Berger. D., *Ordered mesoporous silica and aluminosilicate-type matrix for amikacin delivery systems*, Microporous Mesoporous Mater. 182, **2013**, 32–39

[31] D. Berger, L. Băjenaru, S. Năstase, R.A. Mitran, C. Munteanu, C. Matei, *Influence of structural, textural and surface properties of mesostructured silica and aluminosilicate carriers on aminoglycoside uptake and* in vitro *delivery*, Microporous and Mesoporous Materials, 206, **2015**, 150-160

[32] R. A. Mitran, S. Nastase, C. Stan, A. I. Iorgu, C. Matei, D. Berger, *Doxycycline encapsulation studies into mesoporous SBA-15 silica type carriers and its in vitro release*, 14th International Multidisciplinary Scientific GeoConference on Na Bio and Green: Technologies for Sustainable Future, 1, **2014**, 53-60.

[33] R.A. Mitran, S. Nastase, L. Bajenaru, C. Matei, D. Berger, *Mesostructured Aluminosilicates As Carriers For Doxycycline-Based Drug Delivery Systems*, 14th International Multidisciplinary Scientific GeoConference on Nano, Bio and Green: Technologies for Sustainable Future, 1**, 2014**, 113-120

[34] R. Injac, V. Djordjevic-Milic, B. Srdjenovic, *Thermostability Testing and Degradation Profiles of Doxycycline in Bulk, Tablets, and Capsules by HPLC*, Journal of Chromatographic Science, 45 (9), **2007**, 623-628

[35] K. Kosmidis, P. Argyrakis, P. Machera, *Fractal kinetics in drug release from finite fractal matrices*, The Journal of Chemical Physics, 119 (12), **2003**, 6373-6377

[36] V. Papadopoulou, K. Kosmidis, M. Vlachou, P. Macheras, *On the use of the Weibull function for the discernment of drug release mechanisms*, International Journal of Pharmaceutics, 309 (1–2), **2006**, 44-50

[37] R. A. Mitran, S. Nastase, L. Bajenaru, C. Matei, D. Berger, *Mesostructured Aluminosilicates As Carriers For Doxycycline-Based Drug Delivery Systems*, 14th International Multidisciplinary Scientific GeoConference on Nano, Bio and Green: Technologies for Sustainable Future, 1, **2014**, 113-120

[38] M. Petrescu, R. A. Mitran, A.M. Luchian, C. Matei, D. Berger, *Mesoporous ceria-silica composites as carriers for doxycycline*, UPB Sci Bull., Series B, 77, Iss 3, **2015,** 13-24

[39] Doi, A.M., Stokof, M.K.,*The kinetics of oxytetraciclyne degradation in deionized water under varying temperature pH, light, substrate, and organic matter.,* J.Aquat. Anim. Health 12, **2001**, 246-253

[40] Janssen, A.H., Koster, A.J., de Jong, K.P., *On the shape of the mesopores in zeolite Y: a three-dimensional transmission electron microscopy study combined with texture analysis*, J. Phys. Chem. B 106, **2002**, 11905-11909

[41] M. Petrescu, R.A. Mitran, C. Matei, D. Berger, *Mesoporous silica-ceria composites as carriers for drug delivery systems,* Revue Roumaine de Chimie, 61(6-7), **2016**, 557-563

[42] Martínez, L., Villalobos, R., Sánchez, M., Cruz, J., Ganem, A., Melgoza, L.K., *Monte Carlo simulations for the study of drug release from cylindrical matrix systems with an inert nucleus,* Int. J. Pharm., 369, **2009**, 38-46

[43] Papadopoulou, V., Kosmidis, K., Vlachou, M., Macheras, P., *On the use of the Weibull function for the discernment of drug release mechanism,*Int. J. Pharm., 309, **2006**, 44-50

[44] D. Berger, S. Nastase, R.A. Mitran, M. Petrescu, E. Vasile, C. Matei, T. Negreanu-Pirjol, *Mesostructured silica and aluminosilicate carriers for oxytetracycline delivery systems,* International Journal of Pharmaceutics, 510, **2016**, 524-531

[45] R. A. Mitran, D. Berger, C. Munteanu, C. Matei, *Evaluation of different Mesoporous Silica Supports for Energy Storage in Shape-Stabilized Phase Change Materials with Dual Thermal Responses*, J. Phys. Chem. C., 119, **2015**, 15177-15184

[46] Popa, A. C., Stan, G. E., Enculescu, M., et al. *Superior biofunctionality of dental implant fixtures uniformly coated with durable bioglass films by magnetron sputtering*, Journal of the Mechanical Behavior of Biomedical Materials, 51, **2015,** 313-327

[47] Popa, A. C., Stan, G. E., Besleaga, C., et al., *Submicrometer Hollow Bioglass Cones Deposited by Radio Frequency Magnetron Sputtering: Formation Mechanism, Properties, and Prospective Biomedical Applications*, Acs Applied Materials & Interfaces 8 (7), **2016**, 4357-4367